Nano Research

Open Access

Research Article

Barley leaf-derived extracellular vesicles protect against colitis by targeting retinoic acid metabolism to maintain intestinal epithelial regeneration

Yifan Zhao, Qian Zhao, Wenjing Chen, Liu Yang, Yingzhuo Zhou, Li Dong, Chen Ma, Xiaosong Hu, Fang Chen, Daotong Li ✉, and Yinghua Luo ✉

College of Food Science and Nutritional Engineering, National Engineering Research Center for Fruit and Vegetable Processing, Key Laboratory of Fruits and Vegetables Processing, Ministry of Agriculture, Engineering Research Centre for Fruits and Vegetables Processing, Ministry of Education, China Agricultural University, Beijing 100083, China

Cite this article: *Nano Research*, **2026**, *19*, 94908654. https://doi.org/10.26599/NR.2026.94908654

ABSTRACT: Inflammatory bowel disease (IBD) is a chronic intestinal disorder characterized by barrier dysfunction, for which effective treatments are still lacking. Plant-derived extracellular vesicles represent an emerging class of natural nanotherapeutics. In this study, we isolated and characterized extracellular vesicles from barley leaf (BLEVs), demonstrating typical vesicular morphology with an average diameter of 177 nm and negative surface charge. BLEVs exhibited excellent biosafety, stability, and colon-targeting capability upon oral administration. In mouse models of colitis induced by dextran sulfate sodium or *Citrobacter rodentium*, BLEVs significantly restored intestinal barrier integrity. Using colonic organoids, we further showed that BLEVs promote intestinal stem cell proliferation and epithelial regeneration through activation of the retinoic acid (RA) metabolism pathway. Critically, pharmacological inhibition of retinaldehyde dehydrogenase (RALDH) abolished the protective effects of BLEVs, identifying RALDH as a key molecular target. These findings position BLEVs as a promising therapeutic strategy for IBD, highlighting RA signaling as a potential target for epithelial homeostasis restoration.

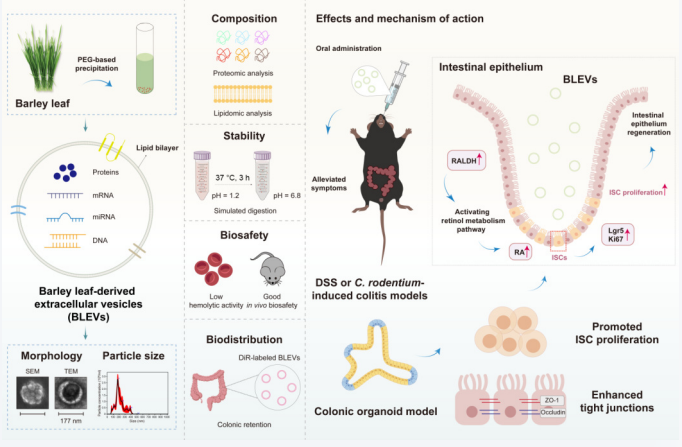

KEYWORDS: inflammatory bowel disease, extracellular vesicles, intestinal barrier, intestinal stem cells, retinoic acid

1 Introduction

Inflammatory bowel disease (IBD), including ulcerative colitis (UC) and Crohn's disease (CD), is a chronic and relapsing inflammation of the intestine affecting millions of people worldwide [1, 2]. The prevalence in western countries, coupled with a rapidly rising incidence in newly industrialized countries, underscores that IBD is becoming a global public health issue [3]. Clinically, patients with IBD exhibit manifestations including recurrent diarrhea, abdominal pain, and body weight loss, which severely affect patients' life quality and impose huge economic burden on healthcare system [4]. Currently, drugs including aminosalicylic acid, mesalamine, sulfasalazine and immunosuppressive agents have been used to treat IBD, but approximately 50% of patients exhibit suboptimal responses to these treatments [5]. Furthermore, the systemic side effects of these medications such as allergic reactions and liver toxicity are limitations for their extensive clinical application [6]. Hence, these drawbacks highlight an unmet need to develop novel and effective approaches for the prevention and treatment of IBD.

Although the pathogenesis is still poorly understood, disruption of the intestinal barrier is a key hallmark of IBD [7]. The intestinal epithelium serves as the fundamental defense line that protects against potentially harmful substances and infectious agents from the gut lumen [8]. The structural integrity of the intestinal epithelium relies on continuous self-renewal and regeneration

Received: January 12, 2026; **Revised:** March 16, 2026
Accepted: March 18, 2026

✉Address correspondence to Daotong Li, lidaotong@cau.edu.cn; Yinghua Luo, luoyinghua@cau.edu.cn

mediated by intestinal stem cells (ISCs) that reside at the base of the intestinal crypt [9]. As a critical regulator of the intestinal homeostasis, ISCs can proliferate and terminally differentiate into enteroendocrine cells, Paneth cells, and goblet cells, which play crucial roles in maintaining intestinal barrier and resisting immune dysregulation [10]. Accumulating evidence has shown that the activity of ISCs is tightly mediated by various factors and signals derived from the host, gut microbiota, and dietary components [11, 12]. Therefore, maintenance of intestinal barrier integrity through regulation of ISCs function may represent a promising strategy for IBD intervention.

Extracellular vesicles (EVs), the lipid bilayer-enclosed nanoparticles released by various cell types, have been identified as important mediators of intercellular communication by carrying cargoes that can deliver signals to recipient cells [13]. A growing body of evidence has highlighted the potential of plant-derived EVs (PDEVs) in treating diverse diseases. Of note, PDEVs offer advantages including improved therapeutic efficacy, desirable bioavailability, biological safety, cost-effectiveness, and high-yield with large-scalability production over mammalian-derived EVs and synthetic nanoparticles [14]. In addition, PDEVs demonstrated remarkable stability in the gastrointestinal environment, facilitating their successful transport and absorption following oral administration [15]. These characteristics indicate that PDEVs hold significant promise as an effective alternative for IBD management.

Barley leaf (BL), the young grass of barley (*Hordeum vulgare* L.), is a natural source of antioxidants, vitamins and minerals, and its juice is widely consumed as a popular healthy beverage in Asian countries [16]. As a traditional Chinese herb, it is historically documented in the "Compendium of Materia Medica" (written by Li Shizhen in 1578) for its medicinal use to relieve chest fullness, clear heat, and improve gut health. Previous studies have revealed its many physiological properties on gastrointestinal functions, such as decreasing the gastrointestinal transit time and increasing the fecal weight [17]. Nevertheless, the biological functions and pharmacological properties of BL-derived extracellular vesicles (BLEVs) have not been studied so far. Whether BLEVs can exert potential therapeutic efficacy in mitigating intestinal inflammation and the detailed mechanisms underlying the impacts of BLEVs on gut health are yet to be elucidated.

In this study, we optimized a differential centrifugation method to perform the first isolation and purification of EVs from BL. We characterized the protein and lipid composition of BLEVs, then evaluated the biosafety and biodistribution *in vivo*. Next, we investigated the therapeutic potentials on colonic inflammation using two experimental colitis models. The biological impacts of BLEVs on preserving intestinal barrier integrity were further explored in *ex vivo* gut organoids. Mechanistically, we demonstrated that BLEVs activated retinol metabolism pathway to increase retinoic acid (RA) synthesis, thereby promoting ISCs-mediated intestinal epithelial development. Overall, this study reveals the potential role of BLEVs in the maintenance of ISCs homeostasis and highlights its translational value as a novel intervention approach for IBD.

2 Results

2.1 Isolation and characterization of BLEVs

In this study, BLEVs were extracted from the juice of fresh BL using an optimized differential centrifugation method as outlined in the schematic diagram (Fig. 1(a)) [18]. Two methods were used to characterize the morphology of BLEVs. The scanning electron microscopy (SEM) observations showed that BLEVs presented spherical shapes with a diameter distribution ranging from 123 to 333 nm (Fig. 1(b)). Transmission electron microscopy (TEM) ultrastructural analysis further confirmed the membrane-enclosed vesicle-like structure of BLEVs, resembling the classic tea tray-like and empty cup-shaped morphology of exosomes (Fig. 1(c)) [19]. Nanoparticle tracking analysis (NTA) demonstrated that the average size distribution of BLEVs was 177 nm (Fig. 1(d)). In addition, the zeta potential measurements showed that the average potential of the particle population was −16.4 ± 0.4 mV, indicating that the vesicles were stable (Fig. 1(e)). The protein concentration of purified BLEVs was quantified using a bicinchoninic acid (BCA) protein assay kit and the results showed that the concentration of fresh BLEVs was about 3.0 mg/mL (Fig. S1 in the Electronic Supplementary Material (ESM)). Collectively, these results demonstrated that we successfully obtained EVs from BL through this optimized protocol.

Proteomic analysis was performed to compare the protein profile of BLEVs with that of the parent leaves. Specifically, a total of 7824 proteins were detected from the samples. Of these, an average of 5029 proteins was identified from EVs, less than the 7363 proteins identified from leaves (Fig. S2(a) in the ESM). The principal component analysis (PCA) revealed a significant difference of the protein compositions between BLEVs and the parent leaves (Fig. S2(b) in the ESM). The volcano plot revealed 3952 downregulated and 1220 upregulated proteins in the BLEVs group compared with the BL group (Fig. S2(c) in the ESM). The hierarchical clustering heatmap demonstrated a notable disparity in the abundance of these proteins between BLEVs and their parent plant leaves (Fig. S2(d) in the ESM). Subcellular localization analysis was performed to identify the localization of differential proteins within the various subcellular organelles. The result showed that the differential proteins are mainly distributed in cytoplasm (19.54%), chloroplast (15.59%), cell membrane (15.11%), nucleus (14.63%), and mitochondrion (11.01%) (Fig. 1(f)). According to the Gene Ontology (GO) analysis, we confirmed that BLEVs are linked to diverse biological processes, among which the oxidation-reduction process was the most significant accompanied by enrichment of 579 differentially expressed proteins (Fig. 1(g)). In addition, molecular function analysis suggested that the expression of proteins associated with oxidoreductase activity was significantly upregulated in BLEVs (Fig. 1(g)). The results of Kyoto Encyclopedia of Genes and Genomes (KEGG) analysis indicated that the proteins in BLEVs were primarily associated with signaling pathways related to phenylpropanoid biosynthesis, metabolic pathways, and cyanoamino acid metabolism (Fig. S2(e) in the ESM).

To explore the lipid composition of BLEVs, non-targeted lipidomic analysis was performed utilizing a liquid chromatography-mass spectrometry (LC-MS) system. The PCA revealed a distinct lipidomic cluster between the two groups (Fig. S3(a) in the ESM). The volcano plot indicated 1348 downregulated lipids and 10 upregulated lipids in BLEVs compared to the parent leaves (Fig. S3(b) in the ESM). The quantitative analysis separately detected five lipid categories, including fatty acyls, glycerolipids, glycerophospholipids, sphingolipids, and saccharolipids (Fig. 1(h)). The relative proportion of these lipid categories varied between

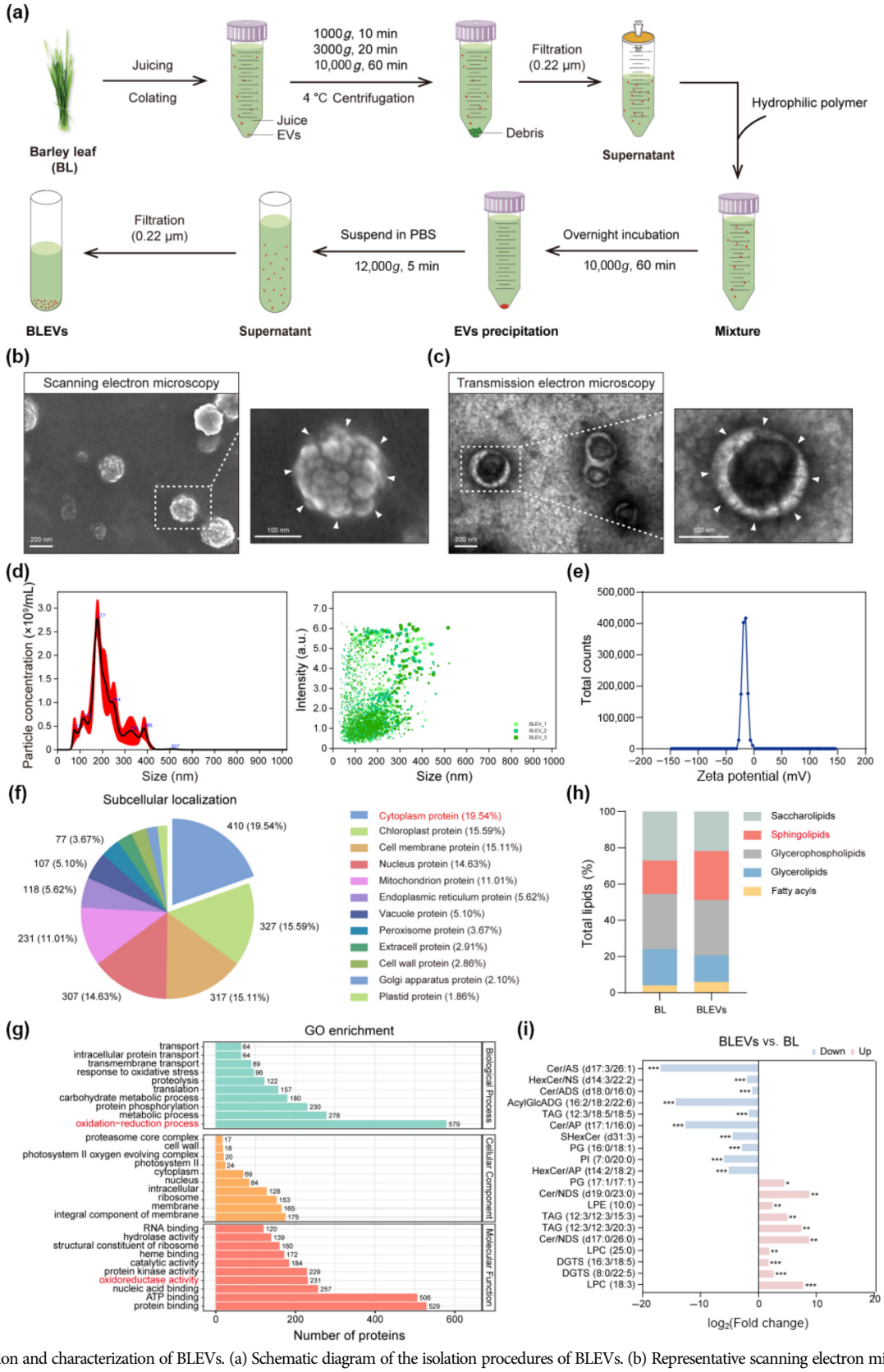

Figure 1 Isolation and characterization of BLEVs. (a) Schematic diagram of the isolation procedures of BLEVs. (b) Representative scanning electron microscopy images of BLEVs. White dotted line marked an EV. Scale bars: 200 nm (left) and 100 nm (right). (c) Representative ultrastructure transmission electron microscopy images of BLEVs. White dotted line marked an EV. Scale bars: 200 nm (left) and 100 nm (right). (d) The average particle concentration and size of BLEVs determined by nanoparticle tracking analysis. (e) Zeta potential values of BLEVs measured using a Zetasizer. (f) Subcellular localization analysis of differentially expressed proteins between BLEVs and BL. (g) GO annotation analysis of differentially expressed proteins between BLEVs and BL. (h) Distribution of major lipid categories isolated from BLEVs and BL. (i) Matchstick analysis of differentially expressed lipids between BLEVs and BL. *$P < 0.05$, **$P < 0.01$, and ***$P < 0.001$.

BLEVs and the parent leaves (Fig. 1(h)). As demonstrated, the proportions of fatty acyls, glycerophospholipids, and saccharolipids remained stable in parent leaves and EVs. Of note, compared to parent leaves (18%), significantly higher ratio of sphingolipids (27%) was identified in BLEVs (Fig. 1(h)). Importantly, sphingolipids were reported to be abundant in the microvillar membrane of intestinal epithelial cells, where they are essential for structural integrity [20]. Furthermore, the hierarchical clustering heatmap displayed a notable disparity in the abundance of lipids between BLEVs and BL (Fig. S3(c) in the ESM). As shown in matchstick analysis, the BLEVs lipid profile exhibited a clear difference from that of parent leaves, as the differential lipids such as ceramide/N-acyl-D-erythro-sphingosine (Cer/NDS), lysophosphatidylcholine (LPC), triacylglycerol (TAG), and other lipid species were significantly upregulated in BLEVs (Fig. 1(i)). Of these lipids, ceramides (Cers), which contain a hydrogen atom as the head group, are the core structures of sphingolipids. It was worth noting that dietary supplementation with plant-derived Cers has demonstrated significant efficacy in ameliorating pathological symptoms in mouse model of IBD [21]. Taken together, these results reveal that BLEVs contain abundant active proteins and lipids, highlighting their potential biomedical applications in IBD therapy.

2.2 BLEVs have favorable biosafety and colonic retention properties

Biosafety is a critical prerequisite for the biomedical applications of BLEVs. We first investigated the hemolytic effect of BLEVs. As shown in Fig. 2(a), no significant hemolysis was observed after incubating red blood cells with different concentrations of BLEVs (10–500 μg/mL), suggesting that BLEVs possess good blood biocompatibility. To determine the biosafety of BLEVs *in vivo*, mice were administered daily with 0.5 and 2.5 mg/kg of BLEVs for 10 days by oral gavage [22, 23]. There were no notable differences in body weight changes and water intake between the BLEVs-treated group and the control group (Figs. 2(b) and 2(c)). Furthermore, histological analysis using hematoxylin and eosin (H&E) staining was performed to assess the impacts of BLEVs on main organs (heart, liver, spleen, lung, kidney and colon) and the results showed no evident abnormalities or organ damage in the BLEVs-treated mice (Fig. 2(d)). Furthermore, blood biochemical analysis including the alanine aminotransferase, aspartate aminotransferase, serum creatinine, and serum urea did not show significant changes between the BLEVs group and the control group (Figs. 2(e)–2(h)).

Given that BLEVs have demonstrated favorable biosafety, we further explored the stability and biodistribution of orally administered BLEVs in mice. First, the stability of BLEVs was evaluated in an *ex vivo* digestive system mimicking the harsh gastrointestinal environment. We incubated BLEVs in simulated gastric fluid at 37 °C for 3 h, followed by simulated intestinal fluid at 37 °C for another 3 h (Fig. S4 in the ESM). TEM imaging indicated that the morphology was well preserved (Fig. S4 in the ESM), indicating that BLEVs can maintain great stability during transit through the gastrointestinal tract. To determine the biodistribution of BLEVs *in vivo*, an infrared fluorescent membrane dye DiR-labeled BLEVs were administered to mice through oral gavage. The fluorescence intensity of DiR-labeled BLEVs in mice was tracked at 3, 6, 12, and 24 h, and recorded employing an *in vivo* imaging technology. Mice receiving equivalent volumes of phosphate-buffered saline (PBS) served as the control group. As shown in Figs. 2(i) and 2(j), DiR-labeled BLEVs were visibly present in the abdominal region at 3 h, and their presence gradually increased at 6 h and steadily decreased by 24 h. In particular, a strong fluorescence signal was clearly detected at the colon within 3 h after the administration (Fig. 2(k)). Moreover, strong fluorescence signals were also detected in the liver, and no obvious fluorescence was found in the heart, spleen, kidney, and lung (Fig. 2(l)). Collectively, these findings indicate that BLEVs are safe and can efficiently accumulate at the colon after oral administration, underscoring their potential application for IBD treatment.

2.3 Oral administration of BLEVs alleviates colitis in mice

To explore whether BLEVs can provide protective effects on mitigating intestinal inflammation, we challenged C57BL/6 mice with free drinking of 2.5% dextran sulfate sodium (DSS) for 7 days to establish a mouse colitis model, which exhibits clinical characteristics resembling patients with UC [24]. During this treatment, colitis mice were orally administered with PBS or BLEVs (0.5 and 2.5 mg/kg per day) (Fig. 3(a)). The mice in DSS group exhibited severe colitis symptoms including significant body weight loss, increased disease activity index (DAI) score, and colon length shortening compared to control group (Figs. 3(b)–3(e)). Of note, the above deleterious effects caused by DSS were attenuated by BLEVs administration (Figs. 3(b)–3(e)). H&E staining and alcian blue (AB) staining were performed on colon tissues to test the effect of BLEVs on intestinal barrier integrity (Figs. 3(f)–3(i)). H&E staining revealed significant pathological changes induced by DSS, including severe colon tissue damage accompanied by crypt deformation, disappearance of goblet cells, and extensive inflammatory cell infiltration (Figs. 3(f) and 3(g)). On the contrary, treatment with BLEVs in DSS-induced colitis mice significantly reversed pathological damage of colon tissue and lowered histopathological scores (Figs. 3(f) and 3(g)). Consistently, AB staining indicated that the number of mucus-producing goblet cells was significantly reduced, and the intestinal mucus barrier was severely compromised in the DSS model group (Figs. 3(h) and 3(i)). However, the intervention of BLEVs effectively alleviated the DSS-induced damage to the mucus barrier (Figs. 3(h) and 3(i)). Additionally, BLEVs also protected against DSS-induced reduction of the tight junction protein ZO-1 in the colons of these mice (Figs. 3(j) and 3(k)). The number of colonic $Ki67^+$ cells was dramatically increased in BLEVs-treated mice (Fig. S5 in the ESM). Consistent with these findings, the serum levels of the proinflammatory cytokines, such as interleukin-6 (IL-6), IL-1β, and tumor necrosis factor-alpha (TNF-α), were suppressed by BLEVs treatment (Figs. 3(l)–3(n)). Together, these results show that BLEVs can alleviate intestinal barrier dysfunction in DSS-induced colitis.

The potential benefits of BLEVs on rescuing intestinal barrier integrity were also verified in the *Citrobacter rodentium* (*C. rodentium*) infection-induced bacterial colitis model [25]. The mice were orally administered BLEVs at different concentrations (0.5 and 2.5 mg/kg per day) once per day for 7 days. On the seventh day, the mice were gavaged with PBS or 1×10^9 CFU of *C. rodentium* (Fig. 4(a)). Similar to the results obtained with DSS-induced colitis, mice that were exposed to a 4-week *C. rodentium* infection suffered from aggressive colitis with bloody diarrhea and rapid loss of body weight, and colon length shortening (Figs. 4(b)–4(e)). Conversely, mice gavaged with BLEVs significantly protected against *C. rodentium*-induced colitis (Figs. 4(b)–4(e)). Histological

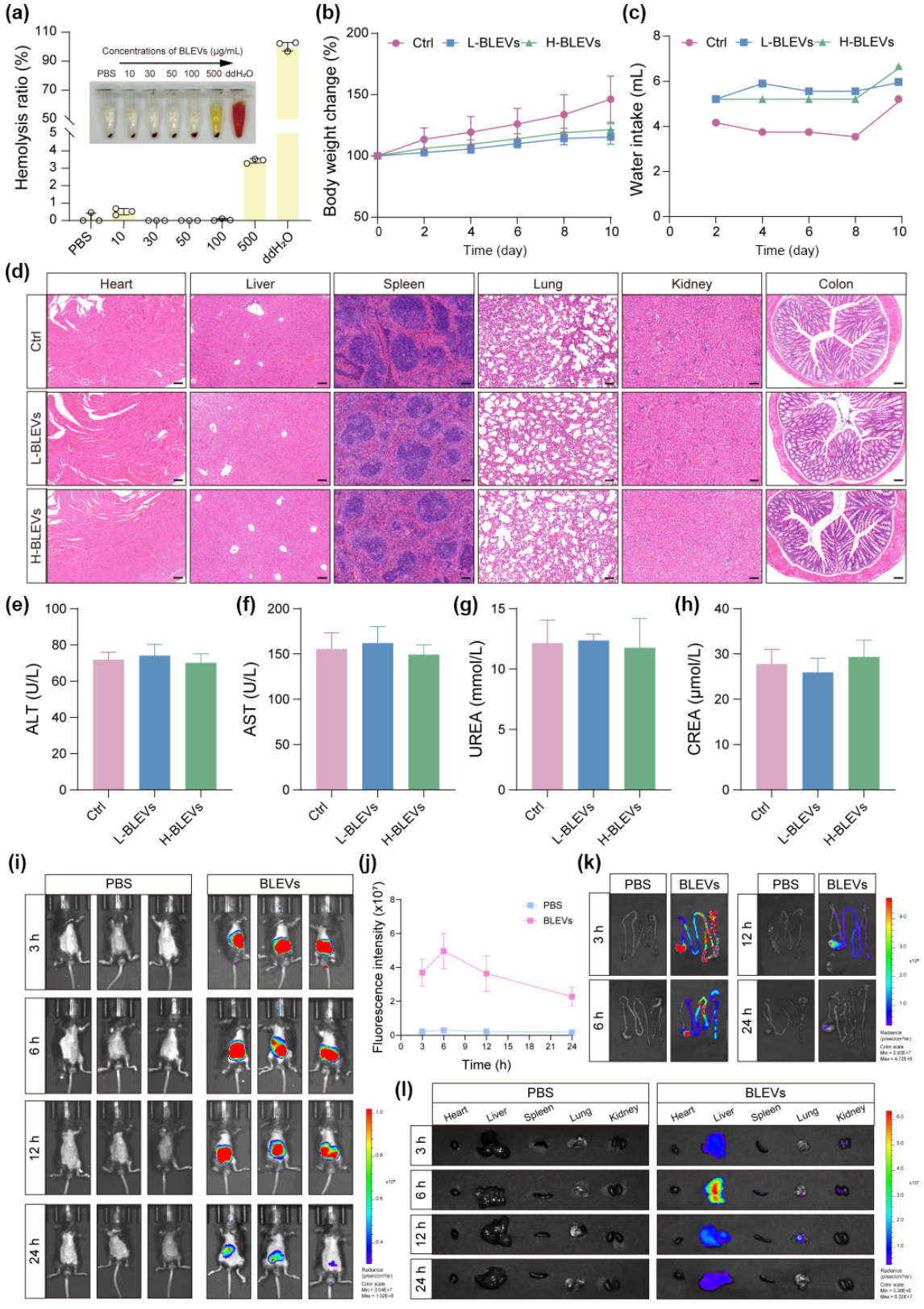

Figure 2 BLEVs show favorable biosafety and colonic retention. (a) Hemolysis activity of BLEVs at different concentrations (n = 3). PBS serves as the negative control while ddH_2O serves as the positive control. *In vivo* biosafety evaluation of BLEVs: Mice were administered daily with L-BLEVs (low dose) and H-BLEVs (high dose) via oral gavage for 10 consecutive days; (b) body weight change, (c) water intake, (d) representative images of H&E-stained liver, heart, spleen, lung, kidneys, and colon tissue slices, scale bars: 100 μm; (e) alanine aminotransferase (ALT), (f) aspartate aminotransferase (AST), (g) urea (UREA), and (h) creatinine (CREA). The stability and biodistribution assays of BLEVs: Mice were administered with DiR-labeled BLEVs via oral gavage; (i) biodistribution of PBS and BLEVs in mice, (j) quantitative analysis of fluorescence intensity in mice, (k) biodistribution of PBS and BLEVs in the gastrointestinal tract, (l) biodistribution of PBS and BLEVs in the heart, liver, spleen, lung, and kidneys at the designated time points after gavage. Data are expressed as mean ± SD.

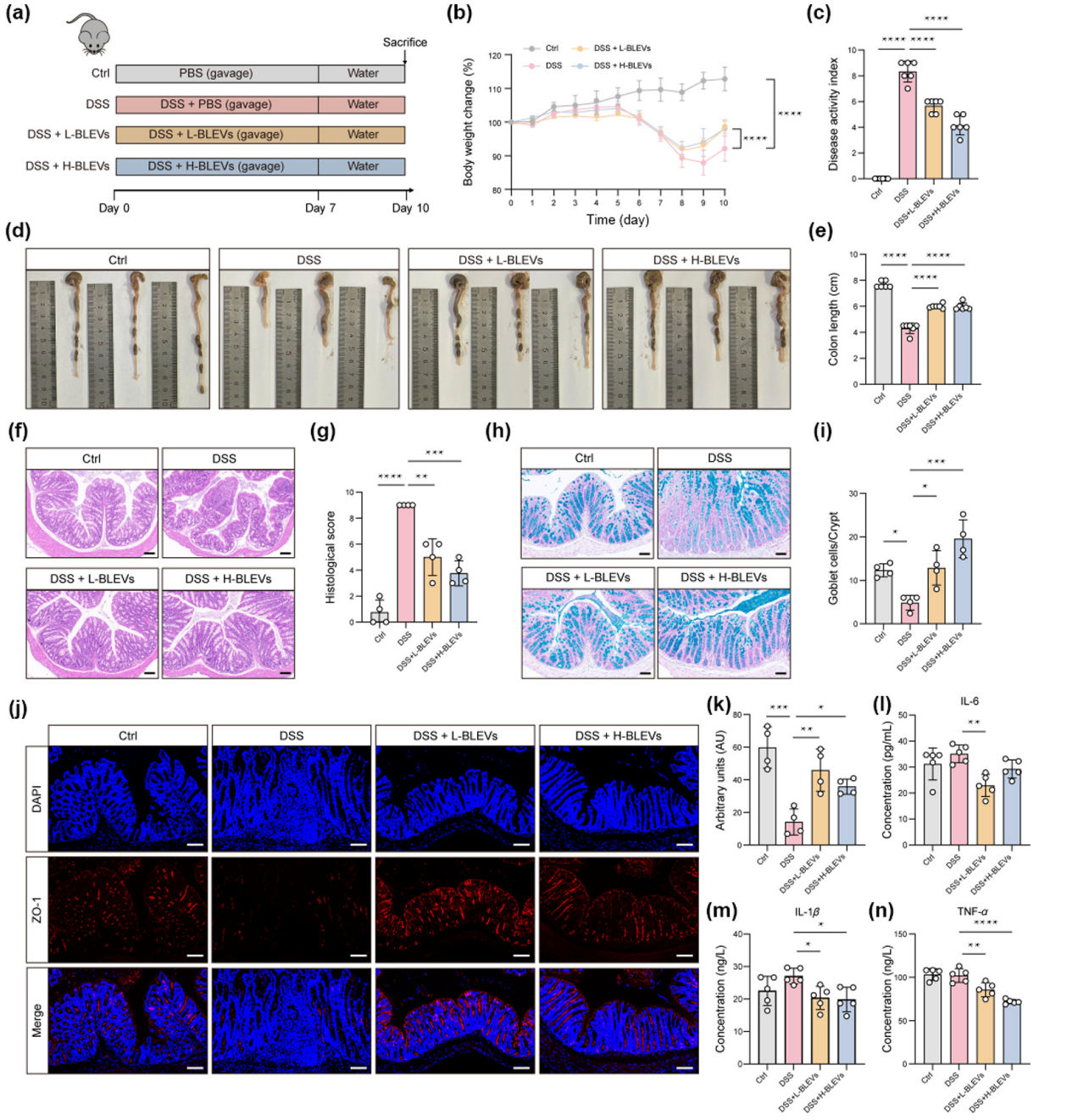

Figure 3 Oral administration of BLEVs alleviates DSS-induced colitis in mice. (a) Diagram of the experimental design. (b) Body weight change. (c) Disease activity index (DAI). (d) Representative colon images and (e) colon length. (f) Representative H&E staining images of colon tissues, scale bars: 100 μm. (g) Histological scores. (h) Representative AB staining images of colon tissues, scale bars: 100 μm. (i) Quantification of goblet cells per crypt. (j) Representative immunofluorescence images of ZO-1 in colonic tissues, scale bars: 100 μm. (k) Quantitative analysis of ZO-1 protein expression in the colon. The serum levels of (l) IL-6, (m) IL-1β, and (n) TNF-α. Data are expressed as mean ± SD. $^{*}P < 0.05$, $^{**}P < 0.01$, $^{***}P < 0.001$, and $^{****}P < 0.0001$.

analysis of colonic sections showed that on day 3 after *C. rodentium* infection led to pathologic changes, such as colonic thickening, mucosal injury, and inflammatory cell infiltration; these histologic damages were remarkably attenuated in BLEVs-treated mice (Figs. 4(f)–4(i)). Moreover, a significant decrease in the level of ZO-1 was observed in *C. rodentium*-infected mice, while BLEVs administration elevated its level in the colon (Figs. 4(j) and 4(k)). The number of colonic Ki67^{+} cells was dramatically increased in BLEVs-treated mice (Figs. S6(a) and S6(b) in the ESM). Consistent with these findings, the serum levels of the proinflammatory cytokines, such as IL-6, IL-1β, and TNF-α, were suppressed by BLEVs treatment (Figs. 4(l)–4(n)). After the oral gavage, *C. rodentium* rapidly established colonization within 24 h after gavage, followed by exponential proliferation in murine gastrointestinal tract, whereas BLEVs exerted significant inhibitory effects on *C. rodentium* growth in the intestinal lumen (Fig. S6(c) in the ESM). Notably, the bacterial levels of *C. rodentium* in spleen and liver were also significantly lower in BLEVs-treated mice (Figs. S6(d) and S6(e) in the ESM), suggesting that BLEVs were able to suppress the systemic diffusion of *C. rodentium* via improved gut barrier

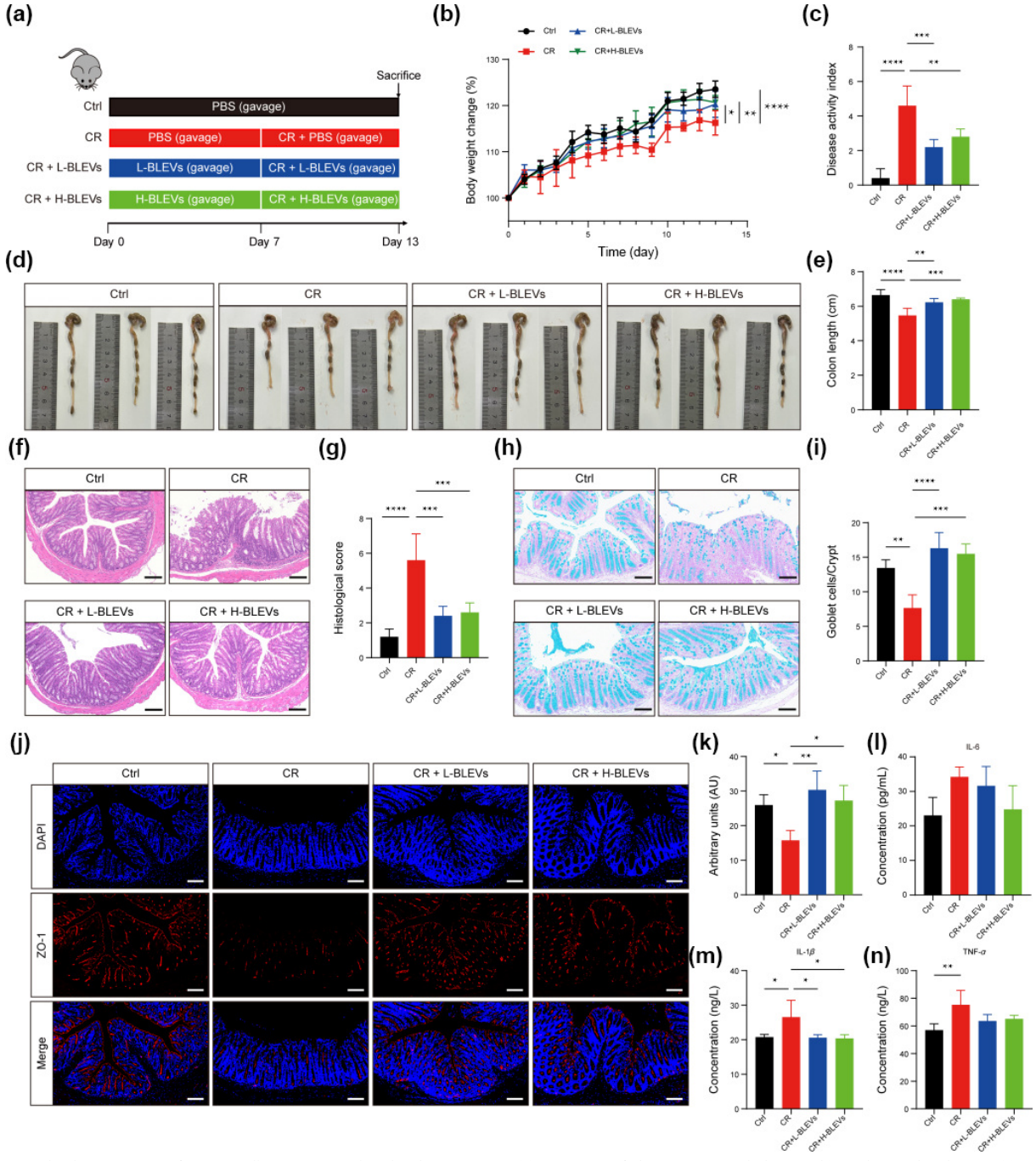

Figure 4 Oral administration of BLEVs alleviates CR-induced colitis in mice. (a) Diagram of the experimental design. (b) Body weight change. (c) DAI. (d) Representative colon images and (e) colon length. (f) Representative H&E staining images of colon tissues, scale bars: 100 μm. (g) Histological scores. (h) Representative AB staining images of colon tissues, scale bars: 100 μm. (i) Quantification of goblet cells per crypt. (j) Representative immunofluorescence images of ZO-1 in colonic tissues, scale bars: 100 μm. (k) Quantitative analysis of ZO-1 protein expression in the colon. The serum levels of (l) IL-6, (m) IL-1β, and (n) TNF-α. Data are expressed as mean ± SD. *$P < 0.05$, **$P < 0.01$, ***$P < 0.001$, and ****$P < 0.0001$.

function. Consistently, the increase of spleen index in *C. rodentium*-infected mice was mitigated (Fig. S6(f) in the ESM). These findings suggest that BLEVs are effective in maintaining intestinal barrier integrity to protect against both chemically- and bacterially-induced colitis.

2.4 BLEVs alleviate DSS-induced intestinal epithelial damage in colonic organoids

Intestinal organoids, which can proliferate and differentiate into all intestinal epithelial cell lines, are an informative *ex vivo* model for studying intestinal barrier function [26]. To further confirm the beneficial role of BLEVs in maintaining intestinal epithelial integrity, we established a DSS-induced intestinal organoids damage model. We first successfully isolated crypts from the colon of mice and cultured them in Matrigel as indicated in the schematic diagram (Fig. 5(a), and Fig. S7 in the ESM). Primary organoids demonstrated characteristic budding structures on the third day (Fig. 5(b)), at which point they were passaged and pre-cultured with

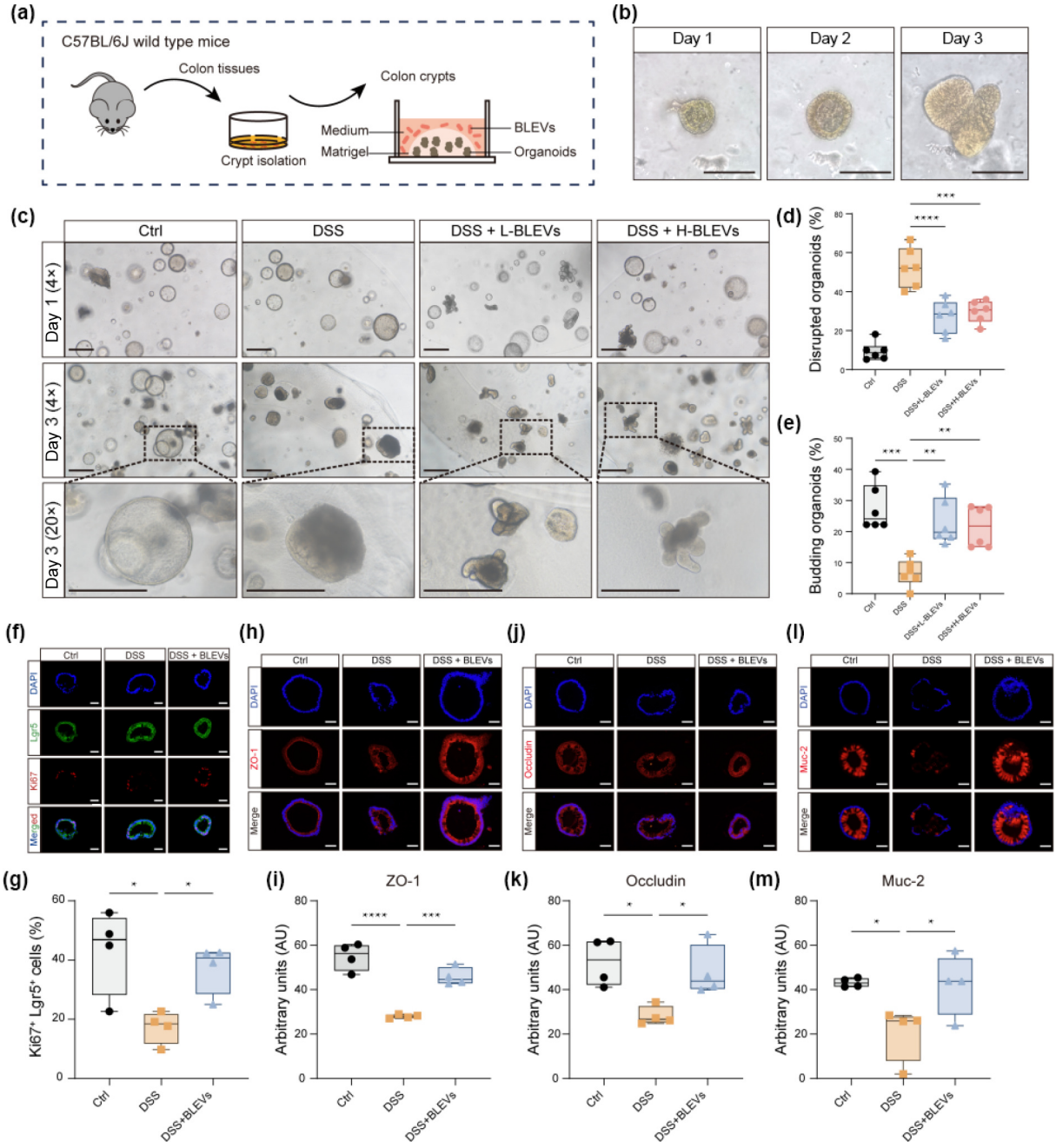

Figure 5 BLEVs alleviate DSS-induced intestinal epithelial damage in colonic organoids. (a) Schematic diagram of colonic organoid culture and treatment. (b) Crypts from colons were seeded onto Matrigel and cultured for 3 days to obtain well-developed organoids, scale bars: 50 μm. (c) Morphology of colonic organoids under white light microscopy in different treatment groups, scale bars: 100 μm. (d) Percentage of disrupted colonic organoids. (e) Budding rate of colonic organoids. (f) Representative immunofluorescence images and (g) quantification of $Lgr5^+$ and $Ki67^+$ cells in colonic organoids. (h) Representative immunofluorescence images and (i) the fluorescence intensities of ZO-1 in colonic organoids. (j) Representative immunofluorescence images and (k) the fluorescence intensities of Occludin in colonic organoids. (l) Representative immunofluorescence images and (m) the fluorescence intensities of Muc-2 in colonic organoids. Data are expressed as mean ± SD. $^*P < 0.05$, $^{**}P < 0.01$, $^{***}P < 0.001$, and $^{****}P < 0.0001$.

BLEVs for 24 h followed by the treatment with 0.1% DSS [27]. After 48 h of exposure to DSS, we observed that approximately half of the organoids exhibited obvious impairment such as shrinkage, darkening and loss of budding structure (Figs. 5(c)–5(e)). However, pretreatment with BLEVs significantly reduced the percentage of disrupted organoids (Figs. 5(c)–5(e)). Immunofluorescence staining against Ki67 and Lgr5 was conducted to evaluate the proliferation status of intestinal epithelial cells. Compared with DSS-treated group, the BLEVs-treated group exhibited a significant increase in the number of proliferating $Lgr5^+$ cells in colonic organoids (Figs. 5(f) and 5(g)). Consistent with a suppressed intestinal epithelial proliferation, we noted that the reduced fluorescence intensity of the tight junction proteins (ZO-1, Occludin) and mucin protein Muc-2 in DSS-treated organoids were significantly improved by BLEVs treatment (Figs. 5(h)–5(m)). Collectively, these data suggest that BLEVs may promote epithelial proliferation and

development to maintain barrier integrity, thereby facilitating the protection against colitis-associated intestinal damage.

2.5 BLEVs promote ISCs-mediated intestinal regeneration by regulating retinol metabolism pathway

As mature intestinal epithelial cells terminally differentiated from ISCs, we next asked whether BLEVs may play a critical role in promoting ISCs-mediated epithelium development under physiological conditions. To address this, we first treated the colonic organoids with BLEVs fluorescently labeled with PKH26 for 24 h. As shown in Fig. 6(a), PKH26-labeled BLEVs were taken up by colonic organoids, indicating a high intracellular uptake efficiency of BLEVs, and this can act as a key step to exert biological function. We next treated colonic organoids with different concentrations of BLEVs (10 and 30 μg/mL) for 24 h. Compared to untreated control group, the budding numbers and surface areas of colonic organoids increased significantly under treatment with BLEVs (Figs. 6(b)–6(d)). The mRNA expression of genes related to ISCs (*Lgr5*) and cell proliferation (*Ki67*) was significantly upregulated in BLEVs-treated organoids compared to that in untreated organoids (Figs. 6(e) and 6(f)). Taken together, these data support that BLEVs promote ISCs' proliferation and intestinal

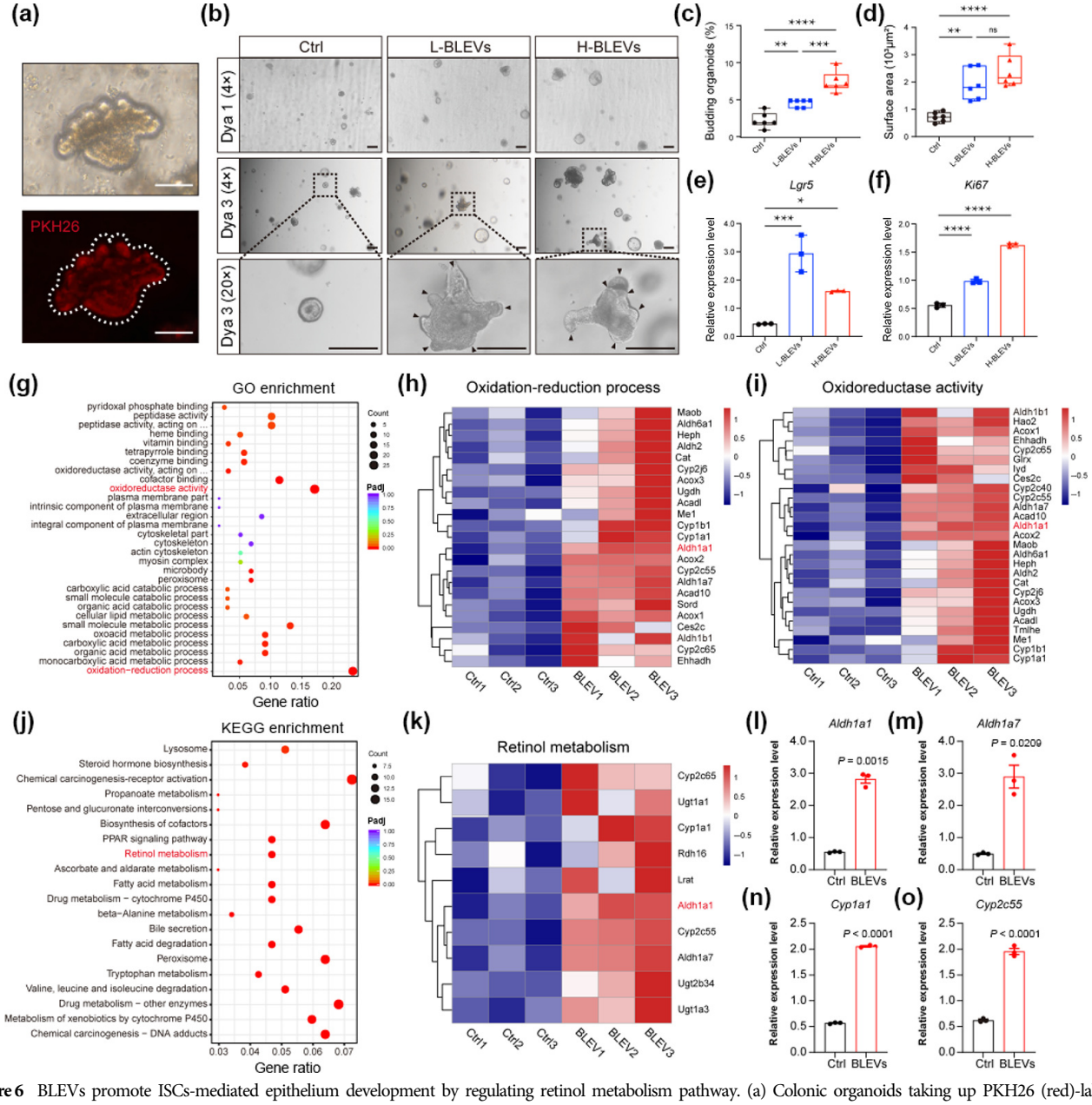

Figure 6 BLEVs promote ISCs-mediated epithelium development by regulating retinol metabolism pathway. (a) Colonic organoids taking up PKH26 (red)-labeled BLEVs, scale bars: 20 μm. (b) Morphology of typical untreated colonic organoids under light microscopy or colonic organoids treated with BLEVs (10 and 30 μg/mL) for 72 h. Budding structures are marked by black triangles, scale bars: 50 μm. (c) Budding rate of colonic organoids. (d) Surface area of colonic organoids. (e) The mRNA expression of *Lgr5*. (f) The mRNA expression of *Ki67*. (g) GO annotation analysis of DEGs between BLEVs and control treatments. (h) Heat map of DEGs in the oxidation-reduction process pathway. (i) Heat map of DEGs in the oxidoreductase activity pathway. (j) KEGG enrichment analysis of DEGs between BLEVs and control treatments. (k) Heat map of DEGs in the retinol metabolism pathway. The mRNA expression levels of the (l) *Aldh1a1*, (m) *Aldh1a7*, (n) *Cyp1a1*, and (o) *Cyp2c55* genes in BLEVs-treated organoids versus control organoids. Data are expressed as mean ± SD. $^{*}P < 0.05$, $^{**}P < 0.01$, $^{***}P < 0.001$, and $^{****}P < 0.0001$; ns: no significance.

epithelial development, thereby accelerating the growth of colonic organoids.

To elucidate the underlying mechanisms by which BLEVs improved ISCs-mediated epithelium development, we performed a comprehensive whole-transcriptome analysis by RNA sequencing on colonic organoids that received a treatment of PBS or BLEVs. PCA revealed significant distinction in the gene expression profiles between the control and BLEVs-treated organoids (Fig. S8(a) in the ESM), which was verified with Pearson correlation analysis (Fig. S8(b) in the ESM). The Venn diagram showed that 297 unique genes were exclusively expressed in the BLEVs group (Fig. S8(c) in the ESM). The volcano plot revealed that BLEVs treatment caused significant down-regulation of 304 genes and up-regulation of 426 genes compared with the control group (Fig. S8(d) in the ESM). GO analysis showed that various biological processes including oxidation-reduction process and oxidoreductase activity were the top significantly influenced pathways by BLEVs treatment (Fig. 6(g)). Interestingly, the genes involved in both the oxidation-reduction process and oxidoreductase activity were primarily associated with genes families encoding retinaldehyde dehydrogenase (RALDH) enzymes, such as *Aldh1a1*, *Aldh1a7*, *Aldh6a1*, *Aldh2*, *Aldh1b1* (Figs. 6(h) and 6(i)). RALDH is a crucial enzyme in retinol metabolism that is involved in the maintenance of intestinal homeostasis [28]. Consistent with these findings, KEGG enrichment analysis showed that the pathway involved in retinol metabolism was significantly enriched by BLEVs treatment (Figs. 6(j) and 6(k)). Furthermore, the upregulated expression of genes involved in retinol metabolism pathway (*Aldh1a1*, *Aldh1a7*, *Cyp1a1* and *Cyp2c55*) was verified by real-time PCR analysis (Figs. 6(l)–6(o)). Collectively, these results suggest that BLEVs promote ISC proliferation and maintain intestinal epithelial development, at least in part, through the regulation of retinol metabolism pathway.

2.6 BLEVs induce RA production and promote intestinal epithelial development through RALDH

In retinol metabolism pathway, RALDH plays a crucial role in the oxidation of retinal, a key step during the synthesis of RA (Fig. 7(a)). RA is a bioactive metabolite of vitamin A and is involved in the regulation of various physiological processes [29]. Recent studies have reported that RALDH plays a crucial role in regulating cell differentiation and has been identified as a marker of stemness in cancer [30–32]. Nevertheless, the biological role for RALDH in promoting ISCs function in colonic organoids has not been reported. We found that the concentration and activity of RALDH but not retinol dehydrogenase (RDH) were increased in colonic organoids following BLEVs treatment (Fig. S9 in the ESM). To determine whether BLEVs promote ISCs-mediated intestinal regeneration through RALDH, we subsequently conducted organoids assays in the presence of 4-diethylaminobenzaldehyde (DEAB), an antagonist of RALDH. Compared to the control group, BLEVs treatment induced a significant increase in the level of RA; however, BLEVs-induced RA production in intestinal organoids was greatly reduced when RALDH was inhibited by DEAB (Fig. 7(b)). Furthermore, BLEVs-treated colonic organoids exhibited a significant increase in the budding numbers and surface areas compared to the control group; notably, this was not seen in organoids treated with DEAB (Figs. 7(c)–7(e)). Consistent with previous results, DEAB treatment eliminated the increased expression of *Aldh1a1*, *Aldh1a7*, and *Cyp2c55*, but not *Cyp1a1* in BLEVs-treated organoids (Figs. 7(f)–7(i)). Consistently, BLEVs failed to increase the expression of ISC marker genes (*Lgr5* and *Ascl2*) and cell proliferation-related genes (*Ki67*, *Axin2*, *Myc*, *Ccnd1*, and *Ctnnb1*) in organoids treated with DEAB (Figs. 7(j) and 7(k)). Collectively, these results indicate that BLEVs promote ISC proliferation and development of intestinal organoids primarily dependent on RALDH.

3 Discussion

IBD is becoming a prevalent global health issue that poses a significant risk to human health [2]. Conventional therapies exhibit limited efficacy and are associated with pronounced side effects [33]. Exploring new intervention strategies with high efficacy and low toxicity for IBD is therefore urgently needed. Our previous studies have demonstrated that dietary supplementation with BL ameliorates experimental colitis by improving gut homeostasis [34, 35]. However, the key functional molecules responsible for the anti-colitis effect of BL and the underlying molecular mechanisms remain to be fully elucidated. Herein, we isolated natural EVs from fresh BL and discovered that BLEVs reach the colon to serve as key bioactive mediators in maintaining intestinal barrier integrity. Mechanistically, we demonstrated that BLEVs could modulate the RALDH-dependent retinol metabolism pathway to promote ISCs regeneration and thereby protect against epithelial barrier damage and colitis progression (Fig. 8).

Emerging evidence has shown that PDEVs display great potential as therapeutic applications in treating various diseases including IBD [36]. For instance, exosome-like nanoparticles derived from medicinal plant *Portulaca oleracea* L. have been found to effectively mitigate colitis symptoms in IL-10$^{-/-}$ mice by reprogramming CD4$^+$ T cells into CD4$^+$CD8$^+$ T cells [37]. Moreover, oral administration of *Momordica charantia*-derived EVs has been shown to alleviate DSS-induced colitis by preventing mitochondrial oxidative damage-dependent apoptosis [38]. In the present study, we successfully extracted and characterized EVs from BL for the first time. Analysis of the physicochemical properties showed that BLEVs have a unique particle size (~ 177 nm) and negative surface charge (−16.4 mV). We evaluated the biological function of BLEVs in mitigating intestinal inflammation. Our study demonstrated that oral administration of BLEVs attenuated both chemically- and bacterially-induced colitis by protecting intestinal barrier integrity. On the basis of proteomic and lipidomic analysis, we found that the enriched proteins and lipids in BLEVs were mainly involved in pathways related to the regulation of redox signaling, which has been reported to be a key regulator of intestinal mucosal homeostasis [39]. Given these insights, we propose that the benefits of BLEVs on attenuating colitis are likely due to the synergistic effects of their biologically active substances.

The biosafety, stability, and biodistribution characteristics of BLEVs were also evaluated. We observed that both low-dose and high-dose BLEVs exhibited no significant hemolysis and good biocompatibility. Notably, BLEVs maintained the structural integrity after 3 h of incubation with simulated gastric and intestinal fluids. Additionally, BLEVs demonstrated prolonged persistence at the colon, thereby enhancing the local bioavailability of their functional cargos. These are consistent with previous findings showing the excellent biosafety and stability of EVs derived from foods, including vegetables, fruits, and milk [40–42]. Collectively, these characteristics provide compelling evidence to support the potential utilization of BLEVs as promising therapeutic agents for IBD management.

The intestinal barrier plays an important role in maintaining

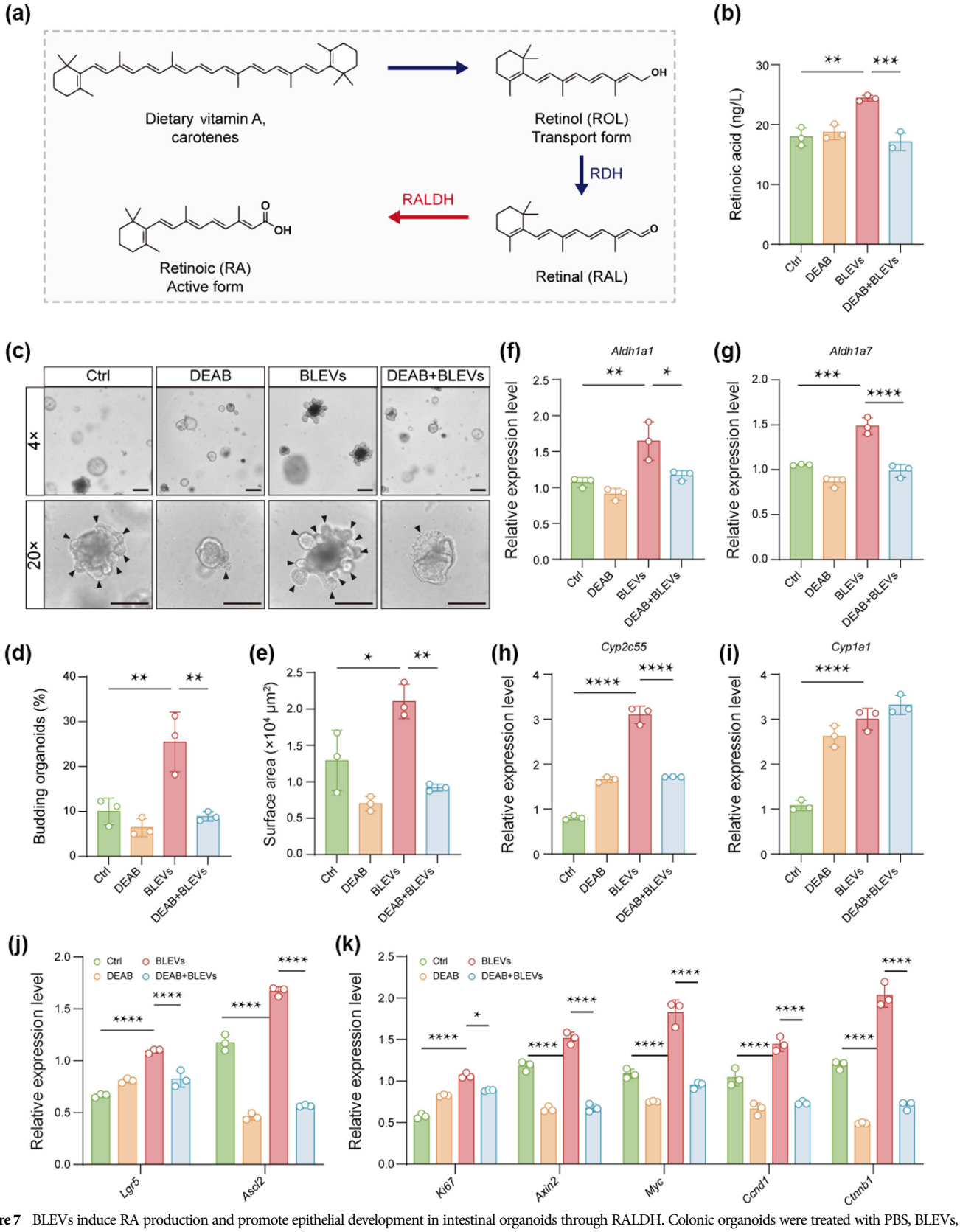

Figure 7 BLEVs induce RA production and promote epithelial development in intestinal organoids through RALDH. Colonic organoids were treated with PBS, BLEVs, DEAB, and DEAB with BLEVs for 72 h. (a) Schematic of retinol metabolism pathway. (b) The concentration of RA in colonic organoids. (c) Representative images of organoids in different treatment groups. Budding structures are marked by black triangles, scale bars: 100 μm. (d) The percentage of budding organoids. (e) The surface area of colonic organoids. The mRNA expression levels of (f) *Aldh1a1*, (g) *Aldh1a7*, (h) *Cyp2c55*, and (i) *Cyp1a1*. (j) The mRNA expression levels of ISC marker genes (*Lgr5* and *Ascl2*). (k) The mRNA expression levels of proliferation-related genes (*Ki67*, *Axin2*, *Myc*, *Ccnd1*, and *Ctnnb1*). Data are expressed as mean ± SD. $^{*}P < 0.05$, $^{**}P < 0.01$, $^{***}P < 0.001$, and $^{****}P < 0.0001$.

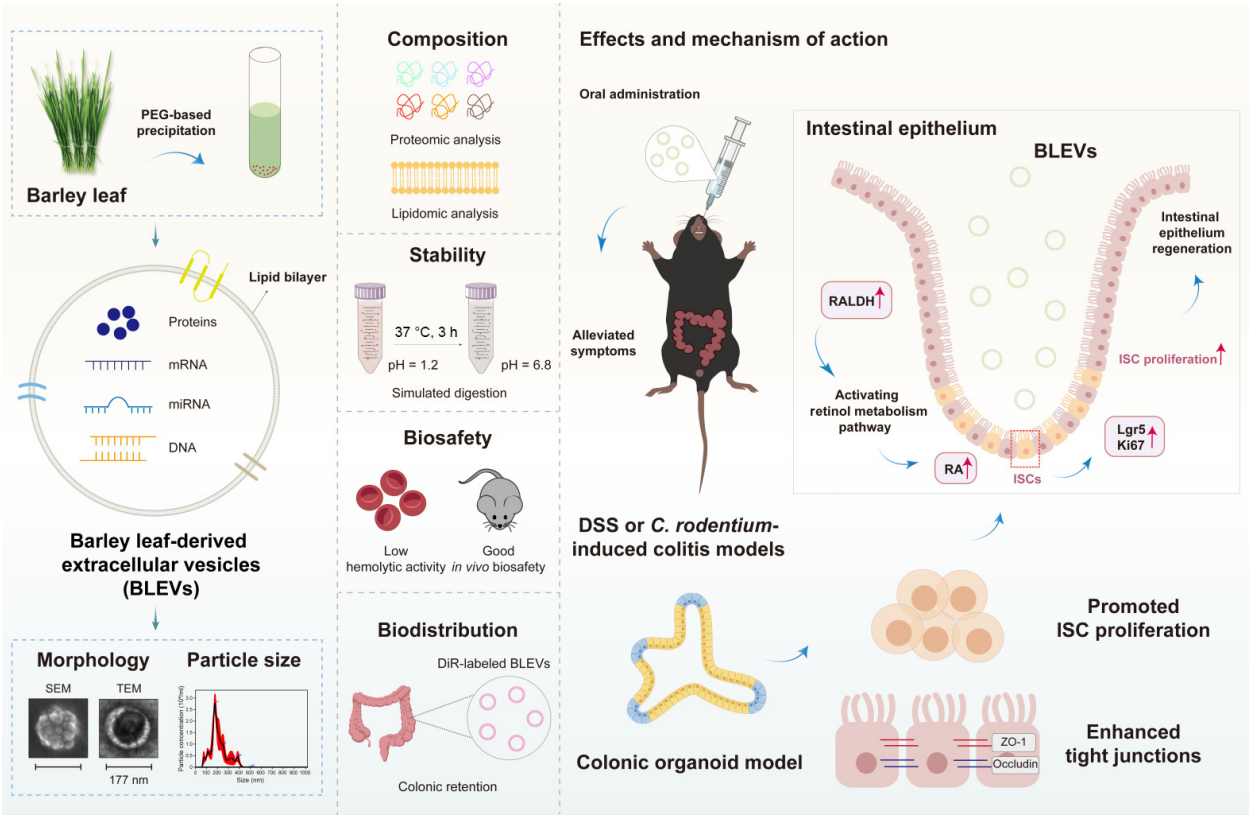

Figure 8 BLEVs promote intestinal epithelial regeneration. Mechanistically, BLEVs significantly enhance the activity of Aldh1a1 (RALDH1), a key enzyme in the retinol metabolism pathway, to increase retinoic acid synthesis, thereby promoting ISC-mediated epithelial renewal and ameliorating gut barrier damage in both DSS- and *C. rodentium*-induced colitis.

mucosal homeostasis [43]. Intestinal barrier dysfunction, characterized by compromised tight junctions and defective mucus layers, is considered as a critical target for IBD therapy [44, 45]. Recent studies have provided evidence showing the applications of PDEVs to improve intestinal barrier function in an *in vitro* cell culturing system. For instance, EVs from orange juice (*Citrus sinensis*) have been shown to counteract the disruption of barrier integrity by increasing the mRNA expression of tight junction proteins in human colonic epithelial cell line Caco-2 [46]. Additionally, garlic-derived exosome-like nanovesicles are able to significantly up-regulate the expression of barrier-related proteins and inhibit the overproduction of pro-inflammatory cytokines in LPS-induced Caco-2 cells [47]. Nevertheless, the traditional use of immortalized intestinal epithelial cell lines, such as Caco-2 cells, cannot accurately recapitulate the real situation of intestinal pathophysiology, showing the limitations in gastrointestinal research. In recent years, the development of intestinal organoid-culturing system has revolutionized the field of stem cell and regenerative research by providing a fundamental preclinical tool for intestinal disease modeling, drug-screening, and translational medical applications [48, 49]. In this study, the 3D colonic organoids were utilized to evaluate the effect of BLEVs on maintaining intestinal barrier integrity. We observed that BLEVs could significantly attenuate DSS-induced organoids damage, further supporting that the improvement of intestinal barrier function contributes to the ameliorating effect of BLEVs on colitis. The immunofluorescence analysis further noted that PKH26-labeled BLEVs could be effectively taken up by the organoids and this is likely attributable to the unique nanosized and lipid membrane-encapsulated structures of PDEVs [50]. Given the favorable uptake characteristics, biosafety and stability, this study also highlights the potential of BLEVs as promising biocompatible drug carriers in treating diseases associated with intestinal barrier dysfunction, which is required to be confirmed in further research.

Residing at the base of the intestinal crypt, ISCs can generate all mature lineages that comprise the intestinal epithelium, thus making them critical therapeutic targets in intestinal diseases [51]. Studies have shown that a highly coordinated proliferation and differentiation of ISCs is essential for the constant turnover and regeneration of the intestinal epithelium, which can be influenced by various factors including dietary components [11]. It has been reported that grape exosome-like nanoparticles can specifically target the $Lgr5^{hi}$ ISCs to mediate intestinal tissue remodeling, thereby protecting against DSS-induced colitis [52]. Consistent with these findings, our data showed that BLEVs were able to increase the budding numbers and surface areas of colonic organoids. Moreover, the increased expression of ISCs marker genes (*Lgr5*) and cell proliferation-related genes (*Ki67*) further confirmed that BLEVs possess the potential of enhancing ISCs function and epithelial development.

Further investigations were conducted to decipher the mechanisms underlying the effect of BLEVs on promoting the growth of intestinal organoids. RNA sequencing analysis showed that the retinol metabolism pathway was significantly enriched in BLEVs-treated organoids. In retinol metabolism pathway, vitamin A serves as an important substrate to generate the active metabolite RA via a two-step dehydrogenation reaction [53, 54]. RALDH, encoded by the *Aldh1a* gene families, is the key enzyme involved in

the conversion of retinal to RA. It has been reported that the intestinal epithelial cells efficiently synthesize RA by expressing the critical enzyme RALDH1, while RALDH2 is mainly expressed in immune cells [55, 56]. In our study, *Aldh1a1* was identified as the core gene in the retinol metabolism pathway and the level of RA was elevated in organoids following BLEVs intervention, suggesting that BLEVs might promote ISCs-mediated intestinal epithelial development through RA synthesis. In experimental necrotizing enterocolitis, enteral administration of RA was able to prevent the induction of crypt apoptosis and preserve the proliferative capacity of the crypt-based ISCs [57]. Moreover, RA has also been shown to enhance enterocyte differentiation in murine small intestinal organoids and promote the forming efficiency of human intestinal organoids [53, 58]. In line with these findings, our data showed that inhibition of RALDH by DEAB blocked the beneficial effects of BLEVs on RA synthesis and ISCs function. Therefore, our findings, together with others, suggest the great potential of manipulating RA signaling for improving ISCs-dependent epithelial barrier integrity.

4 Conclusions

In conclusion, we isolated and characterized EVs from BL, and demonstrated for the first time that oral administration of BLEVs effectively attenuated both chemically- and bacterially-induced colitis by improving intestinal barrier integrity. We further revealed that BLEVs possessed the capability to modulate the RA pathway in colonic organoids, thereby promoting ISCs function and protecting against epithelial barrier damage. Most importantly, RALDH was identified as a key regulator contributing to the biological role of BLEVs in ISCs-mediated intestinal regeneration. Our study thus suggests that BLEVs may be useful as a potential nanomedicine for improving and maintaining gut health.

5 Experimental

5.1 Animals

Male C57BL/6J mice were purchased from Vital River Laboratory Animal Technology (Beijing, China). All protocols for animal experimental manipulations were carried out under the institutional guidelines and were approved by the Animal Ethics Committee of China Agricultural University. All mice were maintained under specific-pathogen-free (SPF) conditions with light/dark cycling for 12 h, controlled temperature (22 °C), humidity (55%), and free access to water and food. Prior to the experimental procedures, the mice were allowed to acclimatize to the laboratory environment for at least one week.

5.2 Isolation and purification of BLEVs

Fresh BL samples were supplied by Hebei Biotechnology Co., Ltd. (Jiaxing, China). After being thoroughly washed three times with water and cut into small pieces, the BL samples were homogenized in PBS using a juice extractor (Joyoung Company Limited, China). Subsequently, the raw juice was initially subjected to low-speed centrifugation to eliminate dead cells, cellular debris, large vesicles, and apoptotic vesicles, followed by polyethylene glycol (PEG)-based isolation as reported [18]. Specifically, sequential differential centrifugation steps were performed at 1000*g* for 10 min, 3000*g* for 20 min, and 10,000*g* for 60 min until no visible precipitate remained in the supernatant. The clarified supernatant was filtered through a 0.45 μm membrane (Acrodisc) and then mixed with an equal volume of 30% (w/v) polyethylene glycol 8000 (PEG-8000) in PBS, resulting in a final PEG concentration of 15% (w/v). The mixture was thoroughly homogenized using a vortex mixer (XH-C, Xinchen Co.) for 1 min and incubated statically at 4 °C for at least 12 h to facilitate phase separation. Post-incubation, the mixture was centrifuged at 10,000*g* for 60 min to precipitate EVs, which were then resuspended with pre-cooled 1× PBS and centrifuged at 12,000*g* for 5 min. Further purification was conducted by filtering the supernatant through a 0.22 μm membrane (Acrodisc). Purified EVs were dispensed in sterile centrifuge tubes (Axygen), and the protein concentrations were quantified using a BCA assay kit (Vazyme Biotech Co., Ltd., Nanjing, China). A NanoSight NS300 instrument (Malvern, Westborough, MA, USA) was used to measure particle size and potential of BLEVs as previously described [59].

5.3 TEM

For ultrastructure TEM analysis, 20 μL of the isolated BLEVs was diluted and mixed in 1 mL 1× PBS. Subsequently, 10 μL of diluted sample was fixed on a copper mesh with 1% glutaraldehyde solution and stained with phosphotungstic acid. Finally, the copper mesh was placed under TEM at 80–120 kV to observe the morphology and structure of the extracted BLEVs. Three independent TEM images of BLEVs were captured using an HT7800 cryo-TEM (HITACHI, Tokyo, Japan).

5.4 SEM

For SEM imaging, BLEVs were fixed on a coverslip pre-coated with 0.01% poly-L-lysine. A volume of 10 μL of the sample was then applied to the coverslip and incubated at room temperature for 20 min to facilitate BLEV adhesion to the glass surface. Following incubation, BLEVs were fixed by treatment with 2% paraformaldehyde for 20 min. After fixation, the sample was washed three times with PBS. The dried sample was attached to a silicon wafer using conductive tape and mounted on the sample holder. The sample was sputter-coated with gold at 10 mA for 80 s before being observed under the SEM to analyze its surface morphology. The SEM images of BLEVs were obtained using a Regulus 8100 SEM (HITACHI, Tokyo, Japan).

5.5 Proteomic and lipidomic analysis

The samples of BLEVs and BL were submitted to Novogene Co., Ltd. (Beijing, China) for proteomic analysis. Specifically, proteins were extracted from both samples and subjected to enzymatic digestion, followed by analysis and identification using LC-MS/MS. The DIA-NN software was employed for library identification and quantitative analysis. The obtained BLEVs and fresh BL samples were sent to Biotree (Shanghai, China) for lipidomic assays. For the isolated lipid metabolites derived from BLEVs and BL, LC-MS/MS analyses were performed using a UHPLC system (Vanquish, Thermo Fisher Scientific) with a Phenomenex Kinetex C18 (2.1 mm × 100 mm, 2.6 μm) coupled to an Orbitrap Exploris 120 mass spectrometer (Orbitrap MS, Thermo). Mobile phase A consisted of H_2O/ACN (6:4, v/v) with 10 mM ammonium formate ($HCOONH_4$), and mobile phase B consisted of IPA/ACN (9:1, v/v) with 10 mM $HCOONH_4$. The injection volume was 2 μL. The Orbitrap Exploris 120 mass spectrometer was used for its ability to acquire MS/MS spectra under the control of the acquisition software (Xcalibur, Thermo). In this mode, the acquisition software continuously evaluates the full scan MS spectrum. The ESI source

conditions were set as follows: sheath gas flow rate 30 Arb, auxiliary gas flow rate 10 Arb, capillary temperature 320 °C, full MS resolution 60,000, MS/MS resolution 15,000, collision energy SNCE 15/30/45, spray voltage 3.8 kV (positive) or −3.4 kV (negative), respectively.

5.6 Hemolysis assay

Fresh whole blood from mice was collected in EDTA tubes containing anticoagulants and gently mixed to ensure homogeneity. The blood was centrifuged at 3000 rpm for 15 min, and the supernatant was collected for detection of pro-inflammatory cytokine levels. The red blood cell pellet was resuspended in PBS, followed by repeated centrifugation under the same conditions (three washes) until the supernatant became clear. A 4% erythrocyte suspension was prepared using PBS/normal saline and stored at 4 °C for subsequent use. Experimental groups included a positive control (Triton X-100), a negative control (PBS), and BLEVs-treated groups with concentrations of 0, 10, 50, 100, 500, and 1000 μg/mL. For testing, 500 μL of erythrocyte suspension was mixed with 500 μL of the corresponding treatment solution. After incubation at 37 °C for 1 h, the mixtures were centrifuged at 2000 rpm for 5 min. The absorbance of the supernatant was measured at 540 nm using a microplate reader. The hemolysis rate was calculated using the following formula [60]: Hemolysis rate (%) = $(OD_{test\ group} - OD_{negative\ control\ group})/(OD_{positive\ control\ group} - OD_{negative\ control\ group}) \times 100\%$.

5.7 Biosafety evaluation

C57BL/6J male mice were randomly divided into three groups: control, L-BLEVs (low dose, gavage), and H-BLEVs (high dose, gavage). The low dose was 10 μg BLEVs per mouse, and the high dose was 50 μg BLEVs per mouse. BLEVs were given every day for 2 weeks. During the entire experiment, the weight, water intake, and food consumption of the mice were recorded every other day. Blood was collected and the serum was isolated for blood biochemistry analysis. Major organs including heart, liver, spleen, lung, kidney and colon were collected for histological examination (H&E staining).

5.8 Stability assay

To evaluate the stability of BLEVs under the gastrointestinal environment, their morphology was monitored by ultrastructure TEM analysis following sequential incubation in simulated digestive fluids. Specifically, the prepared BLEVs were added to simulated gastric fluid (pH = 1.2) and incubated at 37 °C for 3 h, after which samples were collected for TEM characterization. To further simulate digestion from the stomach to the small intestine, the resulting mixture was transferred to simulated intestinal fluid (pH = 6.8) and incubated at 37 °C for another 3 h, followed by sample collection for TEM characterization. The intact morphology observed via TEM demonstrated the remarkable stability and tolerance of BLEVs in the harsh gastrointestinal environment, facilitating their successful transit to the colon following oral administration.

5.9 Biodistribution assay

To evaluate the biodistribution of BLEVs *in vivo*, BLEVs were incubated with the fluorescent dye DiR at 37 °C for 30 min, after which DiR-labeled BLEVs (DiR-BLEVs) were isolated by ultracentrifugation and resuspended in PBS. Six-week-old C57BL/6J male mice were orally administered with DiR-BLEVs. Mice administered PBS served as the control group. At different time points (3, 6, 12, and 24 h), DiR fluorescence was tracked and recorded with an animal *in vivo* imaging system (IVIS SPECTRUM, USA). The mice were euthanized at the designated time points, then the main organs and gastrointestinal tract tissues were imaged by the same imaging system mentioned above.

5.10 Dextran sodium sulfate (DSS)-induced colitis

All mice were adapted to the SPF environment for one week, and then were randomly divided into four groups (n = 6 mice per group): control group (Ctrl), DSS group (DSS), DSS + low-dose BLEVs group (L-BLEVs, 10 μg/day in 200 μL PBS) and DSS + high-dose BLEVs group (H-BLEVs, 50 μg/day in 200 μL PBS). The model was established by free drinking of 2.5% DSS (36–50 kDa, Millipore Corporation, Billerica, MA, USA) for 7 days, while the control group received distilled water. Both the control and DSS groups received sterile PBS via oral gavage. Based on the optimal dosage range of BLEVs determined from preliminary experiments, BLEVs were administered every day to each mouse by gavage. Subsequently, all treatments were replaced with freely available drinking water for the next 3 days. Animal intake and body weight were analyzed every day. On day 10, all mice were euthanized, and blood samples and colonic tissues were rapidly collected for further analysis.

5.11 *Citrobacter rodentium* (*C. rodentium*) infection-induced colitis

After one week of adaptive feeding, male C57BL/6J mice were randomly divided into the Ctrl group, *C. rodentium* group, *C. rodentium* + L-BLEVs group (L-BLEVs, 10 μg/day in 200 μL PBS) and *C. rodentium* + H-BLEVs group (H-BLEVs, 50 μg/day in 200 μL PBS). The Ctrl and *C. rodentium* groups were treated with PBS, while the other groups were treated with L-BLEVs and H-BLEVs, respectively, for 7 days. The mice in each group except for the Ctrl group were gavaged with 1×10^9 CFU of *C. rodentium* for bacterial colitis modeling, and the Ctrl group was given an equal amount of PBS. Throughout the experiment, general health indicators of the mice, including activity, water intake, stool characteristics, and body weight were monitored and recorded daily. Fecal samples were collected at consecutive time points (1, 3, 5 days post *C. rodentium* infection). On day 13, all mice were euthanized, and blood samples, colonic samples, colonic contents, together with liver and spleen, were harvested for subsequent testing.

5.12 Histological analysis

Colon tissues were fixed in 4% paraformaldehyde (Solarbio) and embedded in paraffin. Paraffin-embedded tissue was cut into 5-μm-thick sections and subjected to H&E and AB staining using commercial kits (Beijing Solarbio Technology Co., Ltd., Beijing, China) according to the manufacturer's instructions. Histological staining was quantified using ImageJ software (Media Cybernetics, Inc., Rockville, MD, USA). Four microscopic fields of each section were randomly selected. The histological scores of colonic lesions were calculated according to a previously established scoring system [61], as follows: crypt damage (0–4 scale), severity of inflammation (0–3 scale), and depth of injury (0–3 scale). The mucus-producing goblet cells were observed and counted under a light microscope (Leica DM500).

5.13 Organoids culture and treatment

Colonic organoids were cultured as reported [62]. In brief, colonic tissue specimens were first harvested from healthy male C57BL/6J mice (6–8 weeks old) under sterile conditions. Crypts were isolated via mechanical disruption and enzymatic digestion, including EDTA chelation. Specifically, colonic segments underwent PBS perfusion followed by EDTA-mediated chelation (5 mM) for epithelial detachment, complemented by low-speed shaking at 4 °C for 15 min to enhance crypt dissociation. The resulting crypt fragments were subsequently resuspended in growth factor-reduced Matrigel matrix (#356231, Corning, USA) to establish three-dimensional culture systems. These matrix-embedded crypts were maintained in IntestiCult™ Organoid Growth Medium (#06005, STEMCELL Technologies Inc., Canada), a defined medium formulation containing essential growth factors including R-spondin 1, Noggin, and EGF, which collectively recapitulate the native intestinal stem cell niche. Culture media were refreshed every 48 h to ensure optimal nutrient supply and metabolic waste removal. On the second day, organoids were pretreated with BLEVs (10 or 30 μg/mL) for 24 h, followed by 0.1% DSS exposure. Organoids were treated with BLEVs stained with PKH26 fluorescent dye (Umibio, Shanghai, China) for 12 h to evaluate cellular uptake.

5.14 Immunofluorescence staining

Colonic tissues and organoids were fixed with 4% paraformaldehyde (Solarbio). Samples were cryoprotected with 30% sucrose solution at 4 °C overnight, embedded in OCT compound (Leica), and cryosectioned (5 μm). Organoids or colon sections were incubated in blocking buffer for 1 h before incubation with primary antibodies (ZO-1 (GB12195), Occludin (GB12149), MUC2 (GB120002), Lgr5 (GB112018), and Ki67 (GB111141); all from Servicebio) at 4 °C overnight. After washing, samples were stained with fluorescent dye-conjugated secondary antibodies for 1 h at room temperature and mounted with DAPI. Images were acquired using an eclipse TI2-E inverted research microscope (Nikon) and analyzed with ImageJ software (Media Cybernetics, Inc., Rockville, MD, USA).

5.15 RNA sequencing analysis

Total RNA was extracted from BLEVs-pretreated or control colonic organoids using TRIzol reagent (Invitrogen, USA) according to the manufacturer's instructions. For each group, three independent biological replicates were prepared. RNA concentration and purity were determined prior to sequencing. RNA quality was assessed using the RNA Nano 6000 Assay Kit on an Agilent Bioanalyzer 2100 system (Agilent Technologies, CA, USA). Qualified RNA samples were used for cDNA library construction, followed by high-throughput sequencing performed by SHR-BIO Technologies (Wuxi, China). The libraries were sequenced on an Illumina NovaSeq platform, generating 150 bp paired-end reads, with an average sequencing depth of approximately 20–30 million reads per sample. The raw sequencing data were generated and stored in FASTQ format. To ensure the accuracy and reliability of subsequent bioinformatics analyses, raw sequencing reads were subjected to stringent quality control using the fastp software. Adapter-contaminated sequences, poly-N-containing reads, and low-quality reads were removed using the built-in filtering algorithms of fastp, resulting in high-quality clean reads. Following quality control, key quality metrics of the clean reads were evaluated, including the Q20 and Q30 base quality scores and GC content distribution. The high-quality clean reads were then aligned to the mouse reference genome (GRCm38) using HISAT2 software (v2.0.5) to determine their genomic locations. Gene expression levels were quantified using the featureCounts tool (v1.5.0-p3), which calculates read counts mapped to each gene based on the alignment results.

All downstream sequencing data analyses were performed using R software (v3.6.3). Differentially expressed genes (DEGs) between groups were identified using the DESeq2 R package (v1.20.0). Functional enrichment analyses were subsequently conducted using the clusterProfiler R package, including GO enrichment analysis and KEGG pathway enrichment analysis, to identify significantly enriched biological processes and signaling pathways associated with the DEGs.

5.16 Enzyme-linked immunosorbent assay (ELISA)

Cytokine levels in the colon and RA concentrations in the culture supernatant of colonic organoids were measured using ELISA kits (Jiangsu Meimian Industrial Co., Ltd., Jiangsu, China) following the manufacturer's instructions. Additionally, the protein levels of RDH and RALDH were quantified using corresponding ELISA kits. Briefly, harvested colonic organoids were lysed to obtain total protein extracts, and RDH and RALDH levels were determined according to the manufacturer's protocols.

5.17 RDH and RALDH activity assays

The activities of RDH and RALDH were measured using commercial assay kits (Beijing Solarbio Science & Technology Co., Ltd., Beijing, China) according to the manufacturer's instructions. Briefly, harvested colonic organoids were washed with cold PBS, lysed on ice, and centrifuged (12,000×*g*, 10 min, 4 °C) to obtain protein extracts. The supernatants were collected for enzyme activity analysis, and enzyme activities were normalized to total protein concentrations determined by a BCA assay.

5.18 Quantitative real-time PCR (RT-qPCR)

Total RNA was extracted from mouse colonic organoids using TRIzol reagent (Invitrogen, USA). Subsequently, 1 μg of RNA was reverse transcribed into cDNA following the manufacturer's protocol of the reverse transcription kit (Vazyme, Nanjing, China), which was amplified with SYBR Green Premix ExTaq (Vazyme, Nanjing, China) using a Roche LC480 System. The qPCR reaction conditions were set as follows: predenaturation at 95 °C for 30 s, denaturation at 95 °C for 10 s, and annealing and extension at 60 °C for 30 s, for 40 cycles. Relative gene expression levels were calculated by the $2^{-\Delta\Delta Ct}$ method with GAPDH as the internal reference. Primer sequences are listed in Table S1 in the ESM.

5.19 Statistical analysis

All data are presented as means ± standard deviation (SD). Statistical analysis was conducted using one-way analysis of variance (ANOVA) or Student's *t* test with GraphPad Prism 10.1.2. $P < 0.05$ was considered statistically significant.

Electronic Supplementary Material: Supplementary material (further details of BLEVs proteomics and lipidomics data, supplementary animal experiment data, colonic organoid transcriptomics data, and detailed primer sequences) is available in

the online version of this article at https://doi.org/10.26599/NR.2026.94908654.

Data availability

All data needed to support the conclusions in the paper are presented in the manuscript and/or the Electronic Supplementary Material. Additional data related to this paper may be requested from the corresponding author upon request.

Acknowledgements

All the authors thank the National Engineering Center for Fruits and Vegetables Processing of China Agricultural University for the provision of experimental instruments. We also thank the State Key Laboratory of Natural and Biomimetic Drugs from Peking University Health Science Center for assistance with live imaging of mice. This work is supported by the Chinese National Key Research and Development Program (No. 2023YFF11054005) and the National Natural Science Foundation of China (No. 32371511).

Declaration of competing interest

All the contributing authors report no conflict of interest in this work.

Author contribution statement

Y. F. Z.: Conceptualization, methodology, software, validation, formal analysis, investigation, data curation, writing – original draft, visualization. Q. Z.: Methodology, investigation, data curation. W. J. C.: Methodology, investigation, data curation. L. Y.: Methodology, investigation. Y. Z. Z.: Methodology, investigation. L. D.: Software, formal analysis. C. M.: Software, formal analysis. X. S. H.: Resources, formal analysis. F. C.: Resources, formal analysis. D. T. L. and Y. H. L.: Conceptualization, methodology, resources, data curation, writing – original draft, writing – review & editing, supervision, project administration, funding acquisition. All the authors have approved the final manuscript.

Informed consent

Not applicable.

Ethics statement

The animal experiments were carried out following the guidelines of the China Agricultural University Institutional Committee for the Care and Use of Laboratory Animals and were approved by the Laboratory Animal Welfare and Animal Experimental Ethical Inspection Committee of China Agricultural University (Ethical code: AW82505202-5-01).

Use of AI statement

None.

References

[1] Mehandru, S.; Colombel, J. F. The intestinal barrier, an arbitrator turned provocateur in IBD. *Nat. Rev. Gastroenterol. Hepatol.* **2021**, *18*, 83–84.

[2] Singh, P.; Ananthakrishnan, A.; Ahuja, V. Pivot to Asia: Inflammatory bowel disease burden. *Intest. Res.* **2017**, *15*, 138–141.

[3] Kaplan, G. G.; Ng, S. C. Understanding and preventing the global increase of inflammatory bowel disease. *Gastroenterology* **2017**, *152*, 313–321.e2.

[4] Ouboter, L. F.; Barnhoorn, M. C.; Verspaget, H. W.; Plug, L.; Pool, E. S.; Szuhai, K.; Hawinkels, L. J. A. C.; van Pel, M.; Zwaginga, J. J.; Roelen, D. et al. Local administration of mesenchymal stromal cells is safe and modulates the immune compartment in ulcerative proctitis. *JCI Insight* **2023**, *8*, e167402.

[5] A. P.; Latour, Y. L.; Asim, M.; Barry, D. P.; Allaman, M. M.; Finley, J. L.; Smith, T. M.; McNamara, K. M.; Singh, K.; Sierra, J. C. et al. Protective role of spermidine in colitis and colon carcinogenesis. *Gastroenterology* **2022**, *162*, 813–827. e8.

[6] C. N.; Fried, M.; Krabshuis, J. H.; Cohen, H.; Eliakim, R.; Fedail, S.; Gearry, R.; Goh, K. L.; Hamid, S.; Khan, A. G. et al. World gastroenterology organization practice guidelines for the diagnosis and management of IBD in 2010. *Inflamm. Bowel Dis.* **2010**, *16*, 112–124.

[7] Kong, C.; Yang, M. F.; Yue, N. N.; Zhang, Y.; Tian, C. M.; Wei, D. R.; Shi, R. Y.; Yao, J.; Wang, L. S.; Li, D. F. Restore intestinal barrier integrity: An approach for inflammatory bowel disease therapy. *J. Inflamm. Res.* **2024**, *17*, 5389–5413.

[8] An, J.; Liu, Y. Q.; Wang, Y. Q.; Fan, R.; Hu, X. R.; Zhang, F.; Yang, J. H.; Chen, J. W. The role of intestinal mucosal barrier in autoimmune disease: A potential target. *Front. Immunol.* **2022**, *13*, 871713.

[9] Barker, N.; van Es, J. H.; Kuipers, J.; Kujala, P.; van den Born, M.; Cozijnsen, M.; Haegebarth, A.; Korving, J.; Begthel, H.; Peters, P. J.; Clevers, H. Identification of stem cells in small intestine and colon by marker gene *Lgr5*. *Nature* **2007**, *449*, 1003–1007.

[10] Hou, Q. H.; Ye, L. L.; Huang, L. L.; Yu, Q. H. The research progress on intestinal stem cells and its relationship with intestinal microbiota. *Front. Immunol.* **2017**, *8*, 599.

[11] Shay, J. E. S.; Yilmaz, Ö. H. Dietary and metabolic effects on intestinal stem cells in health and disease. *Nat. Rev. Gastroenterol. Hepatol.* **2025**, *22*, 23–38.

[12] Wu, H. Q.; Mu, C. L.; Xu, L. P.; Yu, K. F.; Shen, L.; Zhu, W. Y. Host-microbiota interaction in intestinal stem cell homeostasis. *Gut Microbes* **2024**, *16*, 2353399.

[13] Cocozza, F.; Grisard, E.; Martin-Jaular, L.; Mathieu, M.; Théry, C. Snapshot: Extracellular vesicles. *Cell* **2020**, *182*, 262–262.e1.

[14] Li, D. F.; Tang, Q.; Yang, M. F.; Xu, H. M.; Zhu, M. Z.; Zhang, Y.; Tian, C. M.; Nie, Y. Q.; Wang, J. Y.; Liang, Y. J. et al. Plant-derived exosomal nanoparticles: Potential therapeutic for inflammatory bowel disease. *Nanoscale Adv.* **2023**, *5*, 3575–3588.

[15] Zhang, M. Z.; Viennois, E.; Prasad, M.; Zhang, Y. C.; Wang, L. X.; Zhang, Z.; Han, M. K.; Xiao, B.; Xu, C. L.; Srinivasan, S. et al. Edible ginger-derived nanoparticles: A novel therapeutic approach for the prevention and treatment of inflammatory bowel disease and colitis-associated cancer. *Biomaterials* **2016**, *101*, 321–340.

[16] Park, M. J.; Seo, W. D.; Kang, Y. H. The antioxidant properties of four Korean barley cultivars at different harvest times and profiling of major metabolites. *J. Agric. Sci.* **2015**, *7*, 94–100.

[17] Ikeguchi, M.; Tsubata, M.; Takano, A.; Kamiya, T.; Takagaki, K.; Ito, H.; Sugawa-Katayama, Y.; Tsuji, H. Effects of young barley leaf powder on gastrointestinal functions in rats and its efficacy-related physicochemical properties. *Evid.-Based Complement. Altern. Med.* **2014**, *2014*, 974840.

[18] Huang, Q. L.; Wang, J.; Ning, H. J.; Liu, W. W.; Han, X. H. Exosome isolation based on polyethylene glycol (PEG): A review. *Mol. Cell. Biochem.* **2025**, *480*, 2847–2861.

[19] Février, B.; Raposo, G. Exosomes: Endosomal-derived vesicles shipping extracellular messages. *Curr. Opin. Cell Biol.* **2004**, *16*, 415–421.

[20] Duan, R.; Nilsson, A. Metabolism of sphingolipids in the gut and its

relation to inflammation and cancer development. *Prog. Lipid Res.* **2009**, *48*, 62–72.

[21] Asanuma, N. Effect of dietary ceramide and glucosylceramide on the alleviation of experimental inflammatory bowel disease in mice. *J. Oleo Sci.* **2022**, *71*, 1397–1402.

[22] Huang, D. F.; Chen, J.; Zhao, M. H.; Shen, H. B.; Jin, Q.; Xiao, D. W.; Peng, Z. B.; Chen, T.; Zhang, Y. L.; Rao, D. Y. et al. Plant-derived extracellular vesicles: Composition, function and clinical potential. *J. Transl. Med.* **2025**, *23*, 1065.

[23] Yang, M.; Guo, J.; Li, J. X.; Wang, S. Y.; Sun, Y.; Liu, Y.; Peng, Y. H. Platycodon grandiflorum-derived extracellular vesicles suppress triple-negative breast cancer growth by reversing the immunosuppressive tumor microenvironment and modulating the gut microbiota. *J. Nanobiotechnol.* **2025**, *23*, 92.

[24] Wirtz, S.; Popp, V.; Kindermann, M.; Gerlach, K.; Weigmann, B.; Fichtner-Feigl, S.; Neurath, M. F. Chemically induced mouse models of acute and chronic intestinal inflammation. *Nat. Protoc.* **2017**, *12*, 1295–1309.

[25] Mullineaux-Sanders, C.; Sanchez-Garrido, J.; Hopkins, E. G. D.; Shenoy, A. R.; Barry, R.; Frankel, G. *Citrobacter rodentium*-host-microbiota interactions: Immunity, bioenergetics and metabolism. *Nat. Rev. Microbiol.* **2019**, *17*, 701–715.

[26] Clevers, H. Modeling development and disease with organoids. *Cell* **2016**, *165*, 1586–1597.

[27] Liang, J.; Dai, W. G.; Liu, C. H.; Wen, Y. F.; Chen, C.; Xu, Y. F.; Huang, S.; Hou, S. Z.; Li, C.; Chen, Y. M. et al. Gingerenone A attenuates ulcerative colitis via targeting IL-17RA to inhibit inflammation and restore intestinal barrier function. *Adv. Sci.* **2024**, *11*, 2400206.

[28] Sanders, T. J.; McCarthy, N. E.; Giles, E. M.; Davidson, K. L. M.; Haltalli, M. L. R.; Hazell, S.; Lindsay, J. O.; Stagg, A. J. Increased production of retinoic acid by intestinal macrophages contributes to their inflammatory phenotype in patients with Crohn's disease. *Gastroenterology* **2014**, *146*, 1278–1288.e2.

[29] Erkelens, M. N.; Mebius, R. E. Retinoic acid and immune homeostasis: A balancing act. *Trends Immunol.* **2017**, *38*, 168–180.

[30] Ciccone, V.; Terzuoli, E.; Donnini, S.; Giachetti, A.; Morbidelli, L.; Ziche, M. Stemness marker ALDH1A1 promotes tumor angiogenesis via retinoic acid/HIF-1α/VEGF signalling in MCF-7 breast cancer cells. *J. Exp. Clin. Cancer Res.* **2018**, *37*, 311.

[31] Ramachandran, I.; Ramadoss, S.; Sen, S.; Karuppaiyah, S.; Kumaran, R. I.; Chaudhuri, G. Inhibition of ALDH1A1 activity in cisplatin-resistant ovarian cancer cells alters their cancer stemness, cell cycle profile and mitochondrial respiration rate. *J. Endocr. Soc.* **2021**, *5*, A1023–A1024.

[32] Szafarowski, T.; Sierdziński, J.; Ludwig, N.; Głuszko, A.; Filipowska, A.; Szczepański, M. J. Assessment of cancer stem cell marker expression in primary head and neck squamous cell carcinoma shows prognostic value for aldehyde dehydrogenase (ALDH1A1). *Eur. J. Pharmacol.* **2020**, *867*, 172837.

[33] Sedano, R.; Almradi, A.; Ma, C.; Jairath, V.; Feagan, B. G. Novel therapeutics for the treatment of IBD: Current status and future directions. *Curr. Treat. Options Gastroenterol.* **2020**, *18*, 442–461.

[34] Feng, Y.; Li, D. T.; Ma, C.; Hu, X. S.; Chen, F. Barley leaf ameliorates *Citrobacter-rodentium*-induced colitis through arginine enrichment. *Nutrients* **2023**, *15*, 1890.

[35] Li, D. T.; Feng, Y.; Tian, M. L.; Ji, J. F.; Hu, X. S.; Chen, F. Gut microbiota-derived inosine from dietary barley leaf supplementation attenuates colitis through PPARγ signaling activation. *Microbiome* **2021**, *9*, 83.

[36] Jung, D.; Kim, N. E.; Kim, S.; Bae, J. H.; Jung, I. Y.; Doh, K. W.; Lee, B.; Kim, D. K.; Cho, Y. E.; Baek, M. C. Plant-derived nanovesicles and therapeutic application. *Pharmacol. Ther.* **2025**, *269*, 108832.

[37] Zhu, M. Z.; Xu, H. M.; Liang, Y. J.; Xu, J.; Yue, N. N.; Zhang, Y.; Tian, C. M.; Yao, J.; Wang, L. S.; Nie, Y. Q. et al. Edible exosome-like nanoparticles from portulaca oleracea L mitigate DSS-induced colitis via facilitating double-positive $CD4^+CD8^+$ T cells expansion. *J. Nanobiotechnol.* **2023**, *21*, 309.

[38] Gao, B. W.; Huang, X. L.; Fu, J. L.; Chen, L. Y.; Deng, Z. C.; Wang, S. H.; Zhu, Y. Y.; Xu, C. X.; Zhang, Y. J.; Zhang, M. X. et al. Oral administration of *Momordica charantia*-derived extracellular vesicles alleviates ulcerative colitis through comprehensive renovation of the intestinal microenvironment. *J. Nanobiotechnol.* **2025**, *23*, 261.

[39] Campbell, E. L.; Colgan, S. P. Control and dysregulation of redox signalling in the gastrointestinal tract. *Nat. Rev. Gastroenterol. Hepatol.* **2019**, *16*, 106–120.

[40] Feng, J. J.; Xiu, Q.; Huang, Y. Y.; Troyer, Z.; Li, B.; Zheng, L. Plant-derived vesicle-like nanoparticles as promising biotherapeutic tools: Present and future. *Adv. Mater.* **2023**, *35*, 2207826.

[41] Teng, Y.; Ren, Y.; Sayed, M.; Hu, X.; Lei, C.; Kumar, A.; Hutchins, E.; Mu, J. Y.; Deng, Z. B.; Luo, C. et al. Plant-derived exosomal microRNAs shape the gut microbiota. *Cell Host Microbe* **2018**, *24*, 637–652.e8.

[42] Tong, L. J.; Zhang, S. T.; Liu, Q. Q.; Huang, C. Y.; Hao, H. N.; Tan, M. S.; Yu, X. D.; Lou, C. K. L.; Huang, R.; Zhang, Z. et al. Milk-derived extracellular vesicles protect intestinal barrier integrity in the gut-liver axis. *Sci. Adv.* **2023**, *9*, eade5041.

[43] Turner, J. R. Intestinal mucosal barrier function in health and disease. *Nat. Rev. Immunol.* **2009**, *9*, 799–809.

[44] Holmberg, F. E. O.; Pedersen, J.; Jørgensen, P.; Soendergaard, C.; Jensen, K. B.; Nielsen, O. H. Intestinal barrier integrity and inflammatory bowel disease: Stem cell-based approaches to regenerate the barrier. *J. Tissue Eng. Regen. Med.* **2018**, *12*, 923–935.

[45] Qiao, Y. R.; He, C. E.; Xia, Y. X.; Ocansey, D. K. W.; Mao, F. Intestinal mucus barrier: A potential therapeutic target for IBD. *Autoimmun. Rev.* **2025**, *24*, 103717.

[46] Bruno, S. P.; Paolini, A.; D'Oria, V.; Sarra, A.; Sennato, S.; Bordi, F.; Masotti, A. Extracellular vesicles derived from *Citrus sinensis* modulate inflammatory genes and tight junctions in a human model of intestinal epithelium. *Front. Nutr.* **2021**, *8*, 778998.

[47] Zhu, Z. Z.; Liao, L. Y.; Gao, M. W.; Liu, Q. Garlic-derived exosome-like nanovesicles alleviate dextran sulphate sodium-induced mouse colitis via the TLR4/MyD88/NF-κB pathway and gut microbiota modulation. *Food Funct.* **2023**, *14*, 7520–7534.

[48] Kollmann, C.; Buerkert, H.; Meir, M.; Richter, K.; Kretzschmar, K.; Flemming, S.; Kelm, M.; Germer, C. T.; Otto, C.; Burkard, N. et al. Human organoids are superior to cell culture models for intestinal barrier research. *Front. Cell Dev. Biol.* **2023**, *11*, 1223032.

[49] Rahmani, S.; Breyner, N. M.; Su, H. M.; Verdu, E. F.; Didar, T. F. Intestinal organoids: A new paradigm for engineering intestinal epithelium *in vitro*. *Biomaterials* **2019**, *194*, 195–214.

[50] Lian, M. Q.; Chng, W. H.; Liang, J.; Yeo, H. Q.; Lee, C. K.; Belaid, M.; Tollemeto, M.; Wacker, M. G.; Czarny, B.; Pastorin, G. Plant-derived extracellular vesicles: Recent advancements and current challenges on their use for biomedical applications. *J. Extracell. Vesicles* **2022**, *11*, 12283.

[51] Choi, J.; Augenlicht, L. H. Intestinal stem cells: Guardians of homeostasis in health and aging amid environmental challenges. *Exp. Mol. Med.* **2024**, *56*, 495–500.

[52] Ju, S. W.; Mu, J. Y.; Dokland, T.; Zhuang, X. Y.; Wang, Q. L.; Jiang, H.; Xiang, X. Y.; Deng, Z. B.; Wang, B. M.; Zhang, L. F. et al. Grape exosome-like nanoparticles induce intestinal stem cells and protect mice from DSS-induced colitis. *Mol. Ther.* **2013**, *21*, 1345–1357.

[53] Qu, N.; Jeffcoat, B.; Maity, P.; Christensen, R. K.; Múnera, J. O. Retinoic acid promotes the *in vitro* growth, patterning and improves the cellular composition of human pluripotent stem-cell-derived intestinal organoids. *Int. J. Mol. Sci.* **2022**, *23*, 8624.

[54] Wu, Y. D.; Huang, T. S.; Li, X. H.; Shen, C. H.; Ren, H. L.; Wang, H. P.; Wu, T.; Fu, X. L.; Deng, S. J.; Feng, Z. Q. et al. Retinol dehydrogenase 10 reduction mediated retinol metabolism disorder promotes diabetic cardiomyopathy in male mice. *Nat. Commun.* **2023**, *14*, 1181.

[55] Coombes, J. L.; Siddiqui, K. R. R.; Arancibia-Cárcamo, C. V.; Hall, J.; Sun, C. M.; Belkaid, Y.; Powrie, F. A functionally specialized population of mucosal CD103$^+$ DCs induces Foxp3$^+$ regulatory T cells via a TGF-β- and retinoic acid-dependent mechanism. *J. Exp. Med.* **2007**, *204*, 1757–1764.

[56] Sun, C. M.; Hall, J. A.; Blank, R. B.; Bouladoux, N.; Oukka, M.; Mora, J. R.; Belkaid, Y. Small intestine lamina propria dendritic cells promote de novo generation of Foxp3 T reg cells via retinoic acid. *J. Exp. Med.* **2007**, *204*, 1775–1785.

[57] Niño, D. F.; Sodhi, C. P.; Egan, C. E.; Zhou, Q. J.; Lin, J.; Lu, P.; Yamaguchi, Y.; Jia, H. P.; Martin, L. Y.; Good, M. et al. Retinoic acid improves incidence and severity of necrotizing enterocolitis by lymphocyte balance restitution and repopulation of LGR5$^+$ intestinal stem cells. *Shock* **2017**, *47*, 22–32.

[58] Lukonin, I.; Serra, D.; Challet Meylan, L.; Volkmann, K.; Baaten, J.; Zhao, R.; Meeusen, S.; Colman, K.; Maurer, F.; Stadler, M. B. et al. Phenotypic landscape of intestinal organoid regeneration. *Nature* **2020**, *586*, 275–280.

[59] Chen, X. Y.; Zhou, Y.; Yu, J. J. Exosome-like nanoparticles from ginger rhizomes inhibited NLRP3 inflammasome activation. *Mol. Pharm.* **2019**, *16*, 2690–2699.

[60] Sæbø, I.; Bjørås, M.; Franzyk, H.; Helgesen, E.; Booth, J. Optimization of the hemolysis assay for the assessment of cytotoxicity. *Int. J. Mol. Sci.* **2023**, *24*, 2914.

[61] Meira, L. B.; Bugni, J. M.; Green, S. L.; Lee, C. W.; Pang, B.; Borenshtein, D.; Rickman, B. H.; Rogers, A. B.; Moroski-Erkul, C. A.; McFaline, J. L. et al. DNA damage induced by chronic inflammation contributes to colon carcinogenesis in mice. *J. Clin. Invest.* **2008**, *118*, 2516–2525.

[62] Zhao, Z. X.; Chen, X. Y.; Dowbaj, A. M.; Sljukic, A.; Bratlie, K.; Lin, L. D.; Fong, E. L. S.; Balachander, G. M.; Chen, Z. W.; Soragni, A. et al. Organoids. *Nat. Rev. Methods Primers* **2022**, *2*, 94.

This is an open access article under the terms of the Creative Commons Attribution 4.0 International License (CC BY 4.0, https://creativecommons.org/licenses/by/4.0/).

© The Author(s) 2026. Published by Tsinghua University Press.